

DESIGN, SYNTHESIS OF FUNCTIONAL LINKER FOR THE CONSTRUCTION OF METAL-ORGANIC FRAMEWORKS (MOFs) AND THEIR APPLICATIONS

M.Sc. Thesis

By
PAWAN KUMAR



**DISCIPLINE OF CHEMISTRY
INDIAN INSTITUTE OF TECHNOLOGY INDORE
JUNE 2019**

DESIGN, SYNTHESIS OF FUNCTIONAL LINKER FOR THE CONSTRUCTION OF METAL-ORGANIC FRAMEWORKS (MOFs) AND THEIR APPLICATIONS

A THESIS

Submitted in partial fulfillment of the requirements for the award of the degree
of
Master of Science

by
PAWAN KUMAR



DISCIPLINE OF CHEMISTRY
INDIAN INSTITUTE OF TECHNOLOGY INDORE
JUNE 2019



INDIAN INSTITUTE OF TECHNOLOGY INDORE

CANDIDATE'S DECLARATION

I hereby certify that the work which is being presented in the thesis entitled **DESIGN, SYNTHESIS OF FUNCTIONAL LINKER FOR THE CONSTRUCTION OF METAL-ORGANIC FRAMEWORKS (MOFs) AND THEIR APPLICATIONS** in the partial fulfillment of the requirements for the award of the degree of **MASTER OF SCIENCE** and submitted in the **DISCIPLINE OF CHEMISTRY, Indian Institute of Technology Indore**, is an authentic record of my own work carried out during the time period from July 2017 to June 2019. Thesis submission under the supervision of Dr. Shaikh M. Mobin, Associate professor Discipline of Chemistry, IIT Indore.

The matter presented in this thesis has not been submitted by me for the award of any other degree of this or any other institute.

**Signature of the student with date
(PAWAN KUMAR)**

This is to certify that the above statement made by the candidate is correct to the best of my/our knowledge.

Signature of the Supervisor of with date
(Dr. Shaikh M. Mobin)

PAWAN KUMAR has successfully given his/her M.Sc. Oral Examination held on

Signature of Supervisor of MSc thesis
Date:

Convener, DPGC
Date:

Signature of PSPC Member
Date:

Signature of PSPC Member
Date:

ACKNOWLEDGEMENTS

This thesis is the end of my trip to the master's degree. This thesis has been revised on how to complement the support and encouragement of many people including my friends, friends, colleagues and various institutions. At the end of my thesis, it is a pleasant task to express my thanks to all those who have contributed in many ways to the success of this study and I made it an unforgettable experience for me. First and foremost I wish to thank my supervisor, Dr. Shaikh M. Mobin. He has been supportive since the days I began working on the lab. Who has reviewed a draft of my text provides important suggestions and asks difficult questions. His knowledge, his valuable advice, his constant motivation, affectionate attitude, understanding, patience and good criticism have greatly improved my experience. Without continuous inspiration, this study could not be completed.

I owe my special thanks to my PSPC committee members Dr. Tushar Kanti Mukharjee, Dr. Bishwarup Pathak and DPGC convener Dr. Sanjay Kumar Singh for their valuable ideas and guidance. And I am highly thankful to our honorable Director Prof. Pradeep Mathur and Head, Discipline of Chemistry, Dr. Amrendra K. Singh for their valuable suggestions that have been very helpful for this study. I would also like to thank all the Faculty, Discipline of chemistry IIT Indore for their humble and supportive gesture. Also, I would like to thank SIC IIT Indore, IIT Kanpur for providing characterization facility.

I am immensely extended my thanks to Dr. Anoop Kumar Gupta who helped me during my whole one year project. And I extended my thanks to my group members Dr. Archana Chaudhary, Dr. Sanjay Kumar Verma, Dr. Mohit Saraf, Mr. Khursheed Ahamad, Ms. Pratibha Kumari, Ms. Shagufi Naz Ansari, Mr. Kaushik Natarajan, Mr. Pranav Tiwari, Ms. Navpreet Kaur, Ms. Topi Ghosh, Ms. Richa Rajak, Ms. Neha Chaudhary, Mr. Ravinder Kumar and all other members for consistent support, broadening transparency and broadening horizons during my project.

I sincerely extended my thanks to all my classmates and I feel deep sense of gratitude to my family for their unconditional love and support during this tenure.

PAWAN KUMAR

Dedicated to my Beloved Family

ABSTRACT

The work described in this thesis concerns the synthesis of 5-(1-oxoisindolin-2-yl)isophthalic acid (H_2L). The H_2L was synthesized by substitution reaction of diethyl-5-aminoisophthalate and 2-(bromomethyl)benzonitrile in acetonitrile solvent (alkaline medium). H_2L has been characterized by 1H , ^{13}C NMR spectroscopy and Mass spectrometry. Further H_2L was utilized with dpe and azodpe co-linker in presence of $Zn(NO_3)_2 \cdot 6H_2O$ under hydrothermal condition gave two novel Zn-CPs (coordination polymers), **IITI-2** and **IITI-3** with 1D and 2D structure, respectively. These two CPs were characterized by single crystal X-ray diffraction (SC-XRD). We further examined the energy storage properties of 2D **IITI-3** through Cyclic Voltammetry (CV).

TABLE OF CONTENTS

LIST OF SCHEMES	xii
LIST OF FIGURES	xiii-xv
LIST OF TABLES	xvi
NOMENCLATURE	xvii
ACRONYMS	xviii-xix
Chapter 1: Introduction	1-16
1.1 Metal-Organic Frameworks/Coordination Polymer	2-3
1.2 Synthesis of Metal-Organic Frameworks	4
1.3 Dimensionality in Metal-Organic Frameworks	4-5
1.3.1 1D Coordination Polymers	5
1.3.2 2D Metal-organic Frameworks	6-7
1.3.3 3D Metal-organic Frameworks	7-9
1.4 Applications of Metal-Organic Frameworks	9
1.4.1 Gas adsorption studies	9-10
1.4.2 Heterogeneous catalytic activity	11-12
1.4.3 Sensing	12-13
1.4.4 Energy Storage	13-15
1.5 Organization of the Thesis	16
Chapter 2: Review of Past and Present Work	17-18
Chapter 3: Experimental section	19-23
3.1 Materials	19
3.2 Methods and instrumentation	19

3.3	Electrochemical measurements	19-20
3.4	X-Ray crystallography	20
3.5	Synthesis of organic Linkers	20
3.5.1	Synthesis of H ₂ L	20-22
3.5.1.1	Synthesis of diethyl 5-((2-cyanobenzyl)amino) isophthalate	21
3.5.1.2	Synthesis of Synthesis of 5-(1-oxoisindolin-2-yl) isophthalic acid	22
3.5.2	Synthesis of CP/MOF	22-23
3.5.2.1	Synthesis of IITI-2	23
3.5.2.2	Synthesis of IITI-3	23
Chapter 4: Result and Discussion		24-35
4.1	Characterization of diethyl-5-((2-cyanobenzyl)amino) isophthalat	24-26
4.1.1	NMR Spectroscopy	25
4.1.2	Mass Spectrometry	26
4.2	Characterization of H ₂ L	26-28
4.2.1	NMR Spectroscopy	27
4.2.2	Mass Spectrometry	28
4.3	Crystal structure of IITI-2	28-29
4.4	Crystal structure of IITI-3	29-31
4.5	Electrochemical energy storage application of IITI -3	31-33
Chapter 5: Conclusions and Scope for Future Work		36-37
APPENDIX A		38-40

REFERENCES

41-48

LIST OF SCHEMES

Scheme 1.	The synthetic scheme for preparation of H ₂ L.	21
Scheme 2.	The synthetic scheme for preparation of IITI-2 and IITI-3.	22

LIST OF FIGURES

Figure 1.1	The components of CPs/MOFs.	3
Figure 1.2	1D coordination polymer motifs generally observed.	5
Figure 1.3	View of 1D zigzag, double helical, and single helical coordination polymers.	6
Figure 1.4	Two dimensional MOFs motifs	6
Figure 1.5	(a) Two-dimensional sheet structure with channels, (b) view of interpenetrated 2D sheets to give the 3D structure and (c) the interpenetration for clarity (different colors for each 2D sheet) in Co(II)-MOF.	7
Figure 1.6	Perspective views of generally occurring secondary building units (SBUs).	8
Figure 1.7	Ball–stick models of Na-MOF1 showing the (a) coordination environment around the Na ion center, Na–Na distance, (b) 3D packing along <i>c</i> -axis, (c) cis-arrangement of three arms of L^{3-} ligand and (d) molecular-drone shape. Hydrogen atoms are removed for clarity. D represents the center core of the metal cluster ring.	8
Figure 1.8	SC-SC Transformation of Na-MOF1 to Na-MOF2.	9
Figure 1.9	(a) Representation of the bipillar-layer frameworks for the systematic modulation of the pores (b) CO_2 adsorption isotherms of 1–3 at 195 K.	10
Figure 1.10	Showing the efficient heterogeneous catalytic activity	

	of LCu' for the one pot synthesis of imidazopyridine derivatives by A ³⁻ coupling reactions and synthesis of coumarin derivatives by Pechmann reaction.	12
Figure 1.11	Schematic of the nitrite sensor.	13
Figure 1.12	A schematic representation of Na/Zn-MOF (1).	15
Figure 1.13	A plausible schematic diagram of the formation of 3 .	15
Figure 4.1	The ¹ H NMR spectrum of diethyl 5-(2-cyanobenzyloxy)isophthalate.	25
Figure 4.2	The ¹³ C NMR spectrum of diethyl 5-(2-cyanobenzyloxy)isophthalate.	25
Figure 4.3	ESI-MS spectrum of diethyl 5-((2-cyanobenzyl)amino)isophthalate.	26
Figure 4.4	The ¹ H NMR spectrum of H ₂ L.	27
Figure 4.5	The ¹³ C NMR spectrum of H ₂ L.	27
Figure 4.6	ESI-MS spectrum of H ₂ L.	28
Figure 4.7	(a) Asymmetric unit of IITI-2, (b) Coordination environment around Zinc ions and (c) perspective view of IITI-2.	29
Figure 4.8	(a) 1-D framework of IITI-2, (b) 2-D framework of IITI-2 formed by hydrogen bonding interactions.	29
Figure 4.9	(a) Asymmetric unit of IITI-3, (b) Coordination environment around Zinc ions and (c) 1-D chain of IITI-3.	30
Figure 4.10	(a) View of 2-D framework of IITI-3, (b) 3-D framework of IITI-3 through hydrogen bonding interactions.	31

Figure 4.11	Comparisons of the CV profiles of bare GCE and IITI-3/GCE at scan rate of 100 mV s^{-1}	32
Figure 4.12	CV profiles of IITI-3/GCE at different scan rates ($10\text{-}500 \text{ mV s}^{-1}$)	33
Figure 4.13	GCD profiles of IITI-3/GCE at different current densities ($6\text{-}12 \text{ A g}^{-1}$). (Electrolyte: $1\text{M Na}_2\text{SO}_4$).	34

LIST OF TABLES

Table 1.	A comparison of the supercapacitor performance of IITI-3 with the previous state-of-the-art MOFs materials.	35
Table A1.	Crystal structure and refinement parameters for IITI-2 and IITI-3.	38
Table A2.	Selected bond distances (Å) and bond angles (°) in IITI-2.	39
Table A3.	Selected bond distances (Å) and bond angles (°) in IITI-3.	40

NOMENCLATURE

μ	mu
π	pi
σ	sigma
v	volume
%	percentage
Θ	theta
λ	lambda
\AA	Angstrom
F	Faraday
s	second
A	Ampere
g	gram
mmol	millimole
mm	millimeter

ACRONYMS

N	Nitrogen
O	Oxygen
C	Carbon
H	Hydrogen
Zn	Zinc
CDCl_3	Deuterated chloroform
DMSO	Dimethyl sulphoxide
dpe	(E)-1,2-di(pyridine-4-yl)ethane
azodpe	(E)-1,2-di(pyridine-4-yl)diazene
H_2O	Water
CH_3CN	Acetonitrile
NaOH	Sodium hydroxide
K_2CO_3	Potassium Carbonate
Na_2SO_4	Sodium Sulphate
ESI-MS	Electron Spray Ionization-Mass Spectrometry
NMR	Nuclear Magnetic Resonance

SC-XRD

Single Crystal X-ray Diffraction

CV

Cyclic Voltammetry

CHAPTER 1

1. Introduction

“Supramolecular chemistry outlined as chemistry on the far side the molecule” **- J. M. Lehn**

Supramolecular chemistry on the so much facet focuses on the chemical systems created of a separate sort of assembled molecular subunits or components. Chemistry of molecular assemblies and of the unit bond', 'the chemistry of the non-covalent bond', 'non-molecular chemistry' there are a unit innumerable method we will outline Supramolecular chemistry. Whereas ancient chemistry focuses on the bond, supramolecular chemistry examines the weaker and reversible noncovalent interactions between molecules. These interactions embrace deliquescent forces, element bonding interactions, electricity effects, metal coordination, pi-pi interactions and van der Waal interactions. Supramolecular chemistry demonstrates some necessary ideas like mobile valency chemistry, molecular self-meeting, host-guest chemistry molecular acknowledgment and automatically self-linked molecular styles. Really its associate knowledge domain science covers the complicated chemical species with their chemical, biological and physical options. Johannes Diderik van der Waals 1st postulate the presence of unit forces in 1873. But Nobel laureate Arminius Emil Fisher discovered supramolecular chemistry with its philosophical roots. This field begins with the selective binding of metallic element cations by natural and artificial macro-cyclic and macro-polycyclic matter, the crown ethers and cryptands however currently it encompasses a massive field say from crown ether to calixarenes, from assembly of artificial polymer, to inorganic primarily based metal-organic frameworks. That's the rationale why it's growing terribly quickly seeking application in varied fields like

applied science, Medicine, Catalysis, knowledge storage, and process similarly as in inexperienced chemistry.

1.1. Metal-Organic Frameworks (MOFs) / Coordination Polymer (CPs)

In terms of strict nomenclature, CPs are approved by IUPAC terminology,[1] but solely containing single-chain polymers and not a pair of dimensional or three dimensional compounds. So the word assignment, there's jointly the systematic naming of these compounds that will would like attention.

CPs square measure relevant to several fields like inorganic chemistry, organic chemistry, biochemistry, pharmacology, electrochemistry having several potential applications and thereby continued to draw in world attention and have evidenced to be one amongst the fascinating topics of analysis thanks to their versatile applications in myriad fields meant for the welfare of grouping. CPs are usually infinite polymeric materials generated from the metal ions or the cluster of metal ions as connectors/nodes and multi-dentate organic bridging ligands as linkers. CP may be a chemical compound with continuance coordination entities extending in one, a pair of and three dimensions. CPs having characteristics features like highly crystalline, highly porous, large internal surface area and regular periodic 2D/3D structures are also known by MOFs or porous coordination polymers (PCPs) that are coordination networks with organic ligand. Since fusion of well-ordered structural styles may produce novel materials having physical and chemical features and such kind of studies may bring perception of the molecular assemblies and their utilities. The design possibilities of these MOFs necessarily depend on the topology of linkers and the coordination tendencies of the metal ions. The characteristics of the organic linkers such as bond angle, rigidity, flexibility, bulkiness,

chirality etc. play crucial roles in dictating the overall topology of the framework. Additionally, the synthetic conditions including solvents, counter-anions, pH, temperature, and so on, also has significant effect on the overall structures of the CPs/MOFs (**Figure 1.1**). The unique features of these materials along with tunable pore size and control over the desired properties encourage an innovative growth at the interface of molecular coordination chemistry and material science.[2-4] The arrangement of individual components with in a material determines its macroscopic properties and function(s). Thus, these materials are showing potential applications in diverse area such as selective gas adsorption,[5-8] molecular storage,[9-12] catalysis,[13-16] sensing and recognition,[17-20] magnetism,[21-24] luminescence,[25,26] charge conduction,[27-29] drug delivery,[30-35] ferroelectricity,[36-40] and so on.

Compared to natural occurring Zeolites, MOFs can be synthesized under relatively mild conditions. Besides, MOFs exhibits a variety of pore surface properties like hydrophilicity/hydrophobicity and chirality through incorporation of organic functional groups into the pore walls [41] compared to other microporous materials, such as activate carbon. For brevity, the introduction is limited to description of MOFs and their uses in the areas relevant to the present thesis and not claimed to be exhaustive.

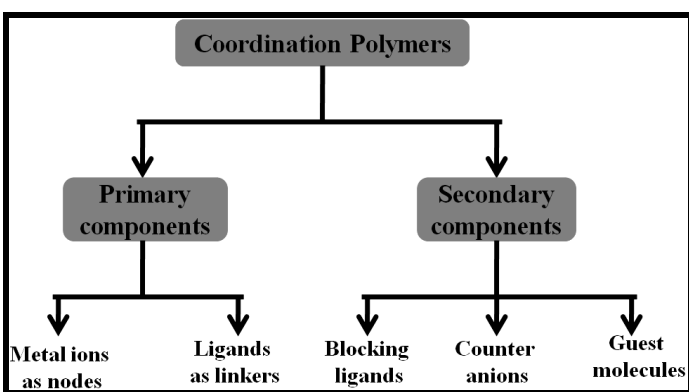


Figure 1.1 The components of CPs/MOFs.

1.2. Synthesis of Metal-Organic Frameworks

MOFs are usually ready by self-assembly, involving crystallization of a metal salt with a substance. The artificial ways utilized to provide coordination polymers square measure typically constant ways wont to grow any crystal. However, the Hydrothermal/Solvothermal methods are generally employed in the synthesis of CPs. Hydrothermal defined that heterogeneous reaction occurs in aqueous solvents under high temperature and pressure. But there is some problem to dissolve the complexes in solution in this method. So, another term comes by chemists, namely Solvothermal which refers that any heterogeneous reaction occurs in presence of non-aqueous (e.g. DMF, DCM, and Methanol) and or aqueous solvents above 1 atm pressure and room temperature in a close system. We carry on this process by a hydrothermal bomb. The MOFs will be synthesized below 250 °C and above this temperature they become porous. Teflon is used as an ideal material to make the hydrothermal bomb. It is chemically inert and resistant to both acidic and alkaline medium. The precursors are usually united as dilute solutions in polar solvents like water, acetone, acetonitrile, or alcohols and heated in sealed vessels that are Teflon-lined chrome steel bombs and making extensive higher pressure to urge a concentrated resolution. Crystal comes out from this solution by cooling. Sometimes mixture of solvent is used to modulate the solvent property and kinetics of solvent ligand exchange.

1.3. Dimensionality in Metal-Organic Frameworks

The crystal construction, assembly and dimensionality of the MOFs/CPs are determined by the linker practicality and also the coordination pure mathematics of the metal center. Dimensionality is usually driven by the metal center which might have the flexibility to bond to as practical sites on linkers. The potential field of solid state architectures and crystal engineering has expanded to the wide variety of

topologies including discrete and infinite one, two and three dimensional (1D, 2D and 3D) networks.

1.3.1. 1D Coordination Polymers

1D CPs are found to be the simplest type of coordination array. Though 1D cycle at least attention-grabbing as compared to the 2D/3D CPs/MOFs, nonetheless they need been found to possess fascinating magnetic, electrical, mechanical and optical properties. A large number of 1D CPs have been reported in the literature. These are mainly classified into zigzag, linear and ladder chains (**Figure 1.2**). Another class of 1D CPs is the helix-type, but it is quite rare in this group.

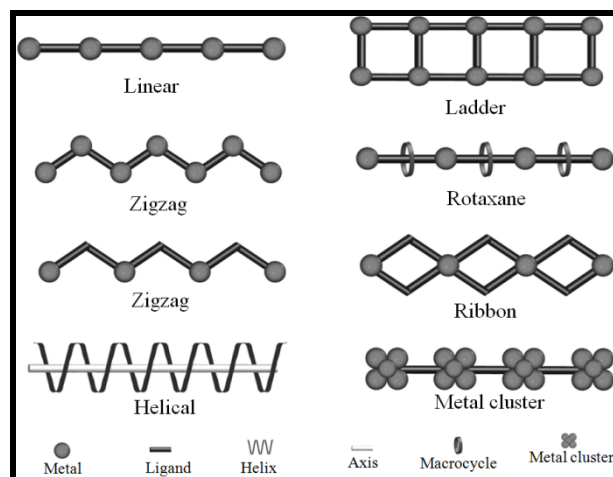


Figure 1.2 1D coordination polymer motifs generally observed.

Lee *et al.* reported three 1D CPs, *viz.* a double helical, a single helical and a zigzag using the conformational effects of 2,6-bis(imidazol-1-yl)pyridine molecule on the self-assembly of infinite chains of Zn(II) below totally fully completely different reaction conditions.[42] Interestingly, when both the single helical and the zigzag polymeric structures are hydrated they exhibit structural transformation to the double helical structure (**Figure. 1.3**).

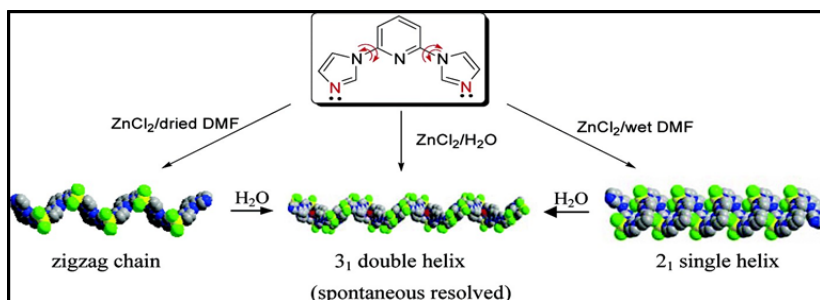


Figure 1.3 View of 1D zigzag, double helical, and single helical coordination polymers.

1.3.2. 2D Metal-organic Frameworks

Two-dimensional MOFs are usually formed when self-assembly facilitates the coordination of three or four ligand moieties as linkers between the metal centers. Most importantly, the other coordination sites of the metal ions are occupied by the counter-anions, solvent molecules or monotopic organic species. Compared to 1D CPs, 2D MOFs are available abundantly in the literature. These 2D coordination complexes show a variety of structures including (a) Herringbone or 'Parquet Floor', (b) Brick Wall, (c) Square Grid, (d) Rectangular grid (e) Honeycomb, (f) Bilayer and so on (**Figure 1.4**).

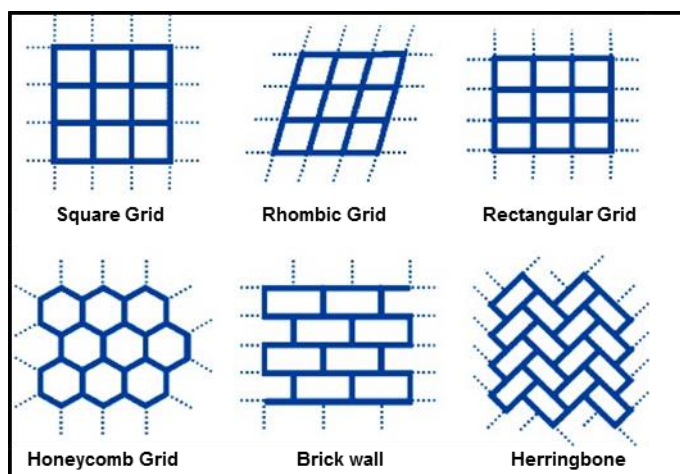


Figure 1.4 Two dimensional MOFs motifs.

Mobin *et al.* reportable a unique two-dimensional (2D) Co(II)-MOF $\{[\text{Co}_5(\text{HL})_4(\text{dpp})_2(\text{H}_2\text{O})_2(\mu\text{-OH})_2] \cdot 21\text{H}_2\text{O}\}_n$ has been designed and

synthesized by adopting a mixed-ligand strategy, using 1,3-di(4-pyridyl)propane (dpp) colinker with a versatile spacer H₃L (H₃L: 5-(2-carboxybenzyloxy)isophthalic acid), CoCl₂·6H₂O in water and NaOH. Co(II)-MOF options a 2nd network, that is any interpenetrated among the equivalent sets and so leads to a 3D supramolecular network (**Figure 1.5**).[43]

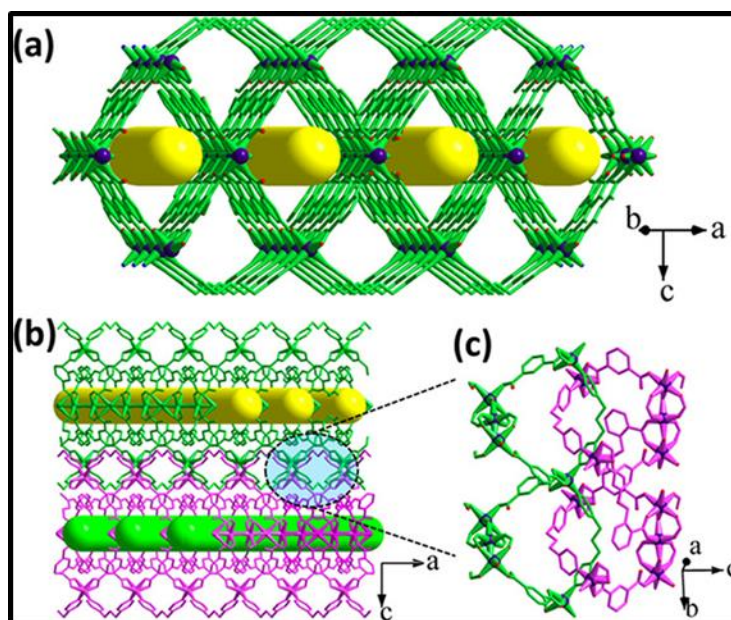


Figure 1.5 (a) Two-dimensional sheet structure with channels, (b) view of interpenetrated 2D sheets to give the 3D structure, and (c) the interpenetration for clarity (different colors for each 2D sheet) in Co(II)-MOF.

1.3.3. 3D Metal-organic Frameworks

3D MOFs are comparatively more porous than 2D. Generally neutral and anion ligands are used to contrast porous 3D MOFs. Neutral ligands decreases the porosity of the framework as anions are trapped inside the cavity that is why anionic ligands are mainly used for highly porous MOFs. Anionic multidentate ligands such as carboxylate allow the formation of metal clusters known as secondary building units (SBU) which is highly rigid in nature (**Figure 1.6**).

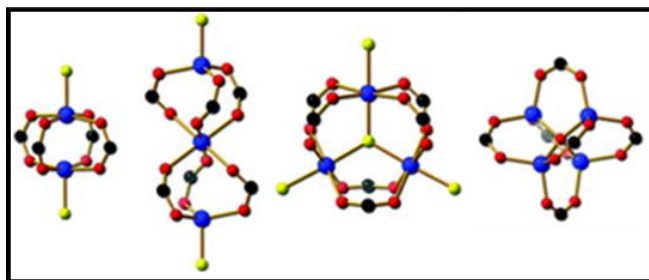


Figure 1.6 Perspective views of generally occurring secondary building units (SBUs).

Mobin *et al.* reported a 3D framework Na-MOF1 that undergoes vacuum-mediated single-crystal-to-single-crystal (SC-SC) transformations (**Figure 1.7**). Further, SC-SC conversion of Na-MOF1 to Na-MOF2 discloses initiation of N–N atoms in 1, 2, 3-triazole unit (**Figure 1.8**). Na-MOF1 and Na-MOF2 were authenticated by single-crystal X-ray studies, and the wholesale was confirmed by powder X-ray diffraction studies.[44]

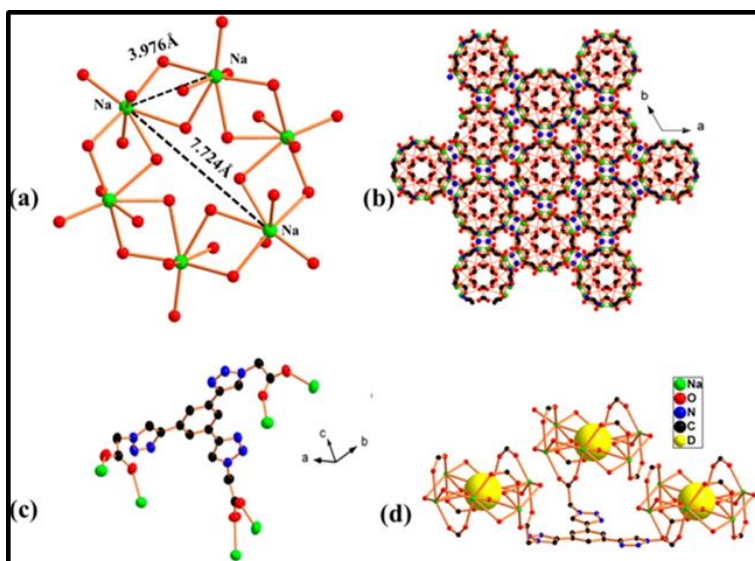


Figure 1.7 Ball–stick models of Na-MOF1 showing the (a) coordination environment around the Na ion center, Na–Na distance, (b) 3D packing along *c*-axis, (c) cis-arrangement of three arms of L^{3-} ligand, and (d) molecular-drone shape. Hydrogen atoms are removed for clarity. D represents the center core of the metal cluster ring.

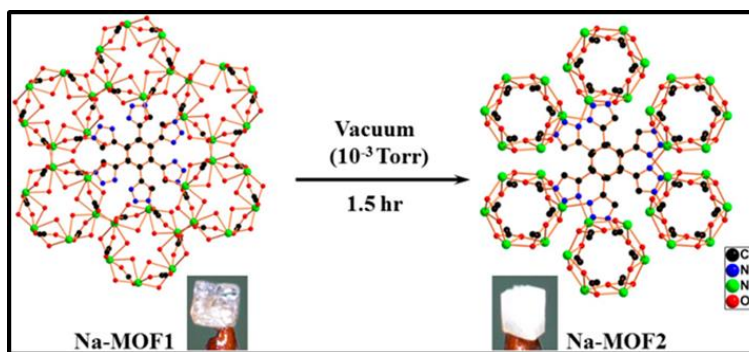


Figure 1.8 SC-SC Transformation of Na-MOF1 to Na-MOF2

1.4. Applications of Metal-Organic Frameworks

Past few decades have witnessed rapid growth in the field of CPs/MOFs due to their potential applications in gas storage, separation, sensing, light harvesting and so on. Among these, MOFs have extraordinarily high surface areas, tunable pore size, and adjustable internal surface properties. These properties along with extraordinary degree of variability for both the organic and inorganic components of their structures make MOFs essential candidates in clean energy, most significantly as storage media for gases such as hydrogen and methane, and as high-capacity adsorbents to meet various separations needs. MOFs are also gaining continuous importance in areas like catalysis, hosting of organic guest molecules, recognition and drug delivery and biomedical imaging. On a fundamental level, MOFs epitomize the beauty of chemical structures and the power of combining organic and inorganic chemistry, two disciplines often regarded as disparate.

1.4.1. Gas adsorption studies

The decreasing amount of relic oils and collective threat of global warming have accelerated research in the field of alternative energy sources as well as flue gas capturing materials. The alternative energy sources hydrogen can be used as an environmentally friendly fuel, which has high energy density with respect to its weight (not in volume though)

in comparison with hydrocarbon fuels. But one of the biggest problems to use hydrogen as a fuel is high energy consumption to store it in compressed form. Other chemical techniques used to store usable hydrogen, such as hydride and amino-borane materials, are also physically and economically demanding processes. So, storing large amount of hydrogen in small volume is an important task. In this context, porous coordination polymers have emerged as one of the most promising adsorbent materials due to their high crystalline nature having microenvironment that could facilitate chemical and physical processes within the confined spaces.

Bharadwaj *et al.* [45] reported a inflexible and bony tetracarboxylic acid 1,3-bis(3,5-dicarboxyphenyl)imidazolium (H_4L^+), joining an imidazolium moiety, has been used with different pyridine-based linkers to form of a sequence of soft cationic frameworks, $\{[Zn_2(L)(bpy)_2] \cdot (NO_3) \cdot (DMF)_6 \cdot (H_2O)_9\}_n$ (1), $\{[Zn_2(L)(dpe)_2] \cdot (NO_3) \cdot (DMF)_3 \cdot (H_2O)_2\}_n$ (2), and $\{[Zn_2(L)(bpb)_2] \cdot (NO_3) \cdot (DMF)_3 \cdot (H_2O)_4\}_n$ (3) bpy = 4,4'-bipyridine, dpe = 1,2-di(4-pyridyl) ethylene, bpb = 1,4-bis(4-pyridyl)benzene. The electronic environment in the frameworks permits choosy CO_2 adsorption above N_2 , where 3 exhibit the maximum selectivity (**Figure 1.9**).

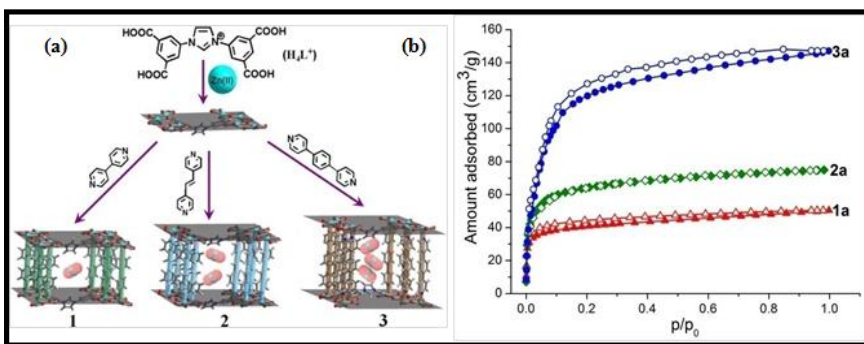


Figure 1.9 (a) Representation of the bipillar-layer frameworks for the systematic modulation of the pores (b) CO_2 adsorption isotherms of 1–3 at 195 K.

1.4.2. Heterogeneous catalytic activity

MOFs like the entrenched microporous zeolites can play a key part in catalyzing many organic transformations. The as-synthesized MOFs may not show any catalytic activities. However, they can be converted into catalytically active materials in several ways. Firstly, there are MOFs where solvent molecules are coordinated to metal ions or metal clusters. On warming these metal bound guest molecules can be eliminated without disturbing the overall framework. This creates open metal sites or unsaturated metal centers that can act as Lewis acid catalysts. MOFs containing metal clusters have also been active this way. Secondly, different functional groups can be covalently attached to the organic linkers such that they decorate the channel surface of the framework. Thirdly, post-synthetic modification of the framework can also be obtained with desirable groups.

Bharadwaj *et al.* synthesized [46] a *NbO* type Homochiral Cu(II)-Metal-organic framework $\{[\text{Cu}_2(\text{L})(\text{H}_2\text{O})_2] \cdot (4\text{DMF})(4\text{H}_2\text{O})\}_n$ (**LCu**) by solvothermal reaction between tetracarboxylate ligand (L=5,5'-(S)-(+)-2-methylpiperazine-1,4-diyl)diisophthalic acid) with copper nitrate. They investigated that the solvent-free framework with unsaturated metal centres (UMCs) (**LCu'**) is a brilliant heterogeneous catalyst for the one-pot synthesis of imidazopyridines through three-component couplings of amines, aldehydes and alkynes as well as the Pechmann condensation reactions to synthesize coumarin derivatives (**Figure 1.10**).

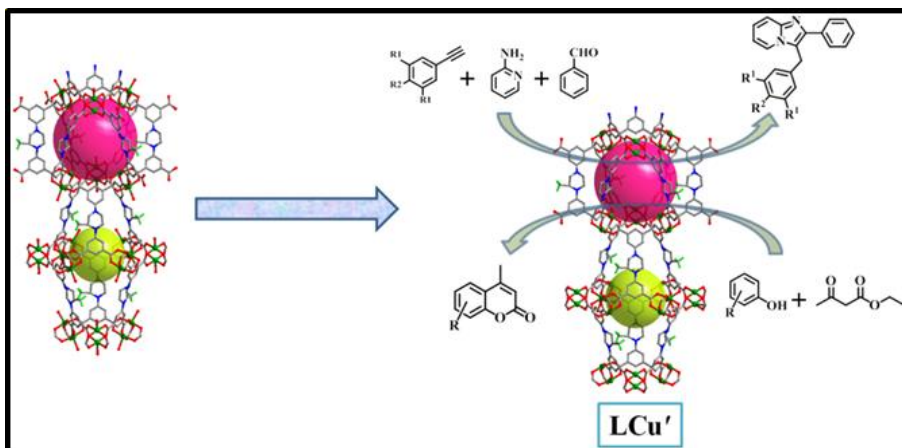


Figure 1.10 Showing the efficient heterogeneous catalytic activity of LCu' for the one pot synthesis of imidazopyridine derivatives by A³-coupling coupling reactions and synthesis of coumarin derivatives by Pechmann reaction.

1.4.3. Sensing

Purely organic and inorganic luminescent material have been extensively explored for their number application lighting, sensing, optical devices and organic light emitting diodes (OLEDs). The assemble of these organic and inorganic component into MOFs or CPs, are the recent kind of organic-inorganic hybrid material provide a platform to generate a luminescent properties. Additionally the metal-ligand charge transfer in the MOF provides extra dimensional luminescent functionalities

Mobin *et al.* fabricated a Cu-MOF/rGO hybrid, by normal ultrasonication of gentle flow focused Cu-MOF crystals with chemically produced rGO. The flexibility of the Cu-MOF/rGO adapted rod can be seen by eminent selectivity in the attendance of some common nose species and also facility to detect nitrite in real examples (**Figure 1.11**).
[47]

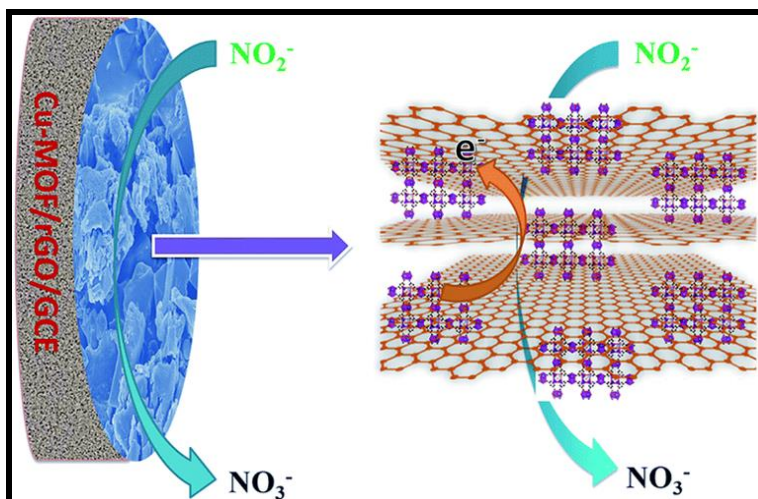


Figure 1.11 Schematic of the nitrite sensor.

1.4.4 Energy Storage

The 2D MOFs have acknowledged an extensive research interest as an innovative participant of the MOF family due to its crystalline structure and layered arrangements, which have an infinite 2D layers adjacent to each other having restacking through strong weak van der Waals forces. These 2D layered constructions allow the firm drive of ions with interpose of electrolyte ions between interlayers of layered crystals. Generally in 3D MOFs, without poor holes providing the loading and transmission of ions, 2D coated MOFs propose interspaces in between layers; hence they can function as electrode materials in supercapacitors. Moreover, the formation of hetero-metallic MOFs can be easily demonstrated by the bimetallic 2D MOFs with absorption of two dissimilar metal ion centers into the same skeleton. This approach results into improved framework strength which provides enhanced performance equated to mono metal MOFs. Though, the arena of supercapacitors built on hetero-metallic MOFs is quiet in the beginning and has enormous possibility. Furthermore, it has not been sometimes witnessed that the low semiconducting of MOFs decays their activity, and there is a need of supplementary conductive additives for complete consumption of composite materials for harmonious approach.

2D paper of reduced graphene oxide (rGO) is an encouraging runner among such materials owing to its covered structure and arrangement, admirable energy storage and great motorized strength. Mixed structure of MOFs and rGO may top to superior potential and also flatten charge movements by giving tiny diffusion channels. Additional benefit of such robust hybrids may be the complete relief from binders, which are commonly used to provide supplementary strength to the composites on surface of electrode. These composites of 2D resources reveal incredible stability and firmness during prolonged cycling, which is very suitable for devices to be used as energy storage. Furthermore, this tactic to create hybrids diminishes the manufacture and fabrication costs, meanwhile such binders are generally pretty expensive. Thus, the formation of composite of two dissimilar 2D layered materials can be a genuine approach to encourage high performance supercapacitor. [48]

Mobin *et al.* reported the simple synthesis of a Na/Zn-based hetero-metallic MOF, $[\text{NaZn}_2(\mu_2\text{-BTC})_2(\mu_2\text{-O})_2(\text{Azopy})(\text{H}_2\text{O})_2]_n$ (**1**) at ambient condition has been grown using a slow dispersal method. The crystal assembly of **1** displays the fraction of 2:1 for Zn(II) and Na(I) ions respectively exhibiting a 2D layered structure in its complete framework (**Figure 1.12**). As already mentioned MOFs generally have poor conductivity, so as to revenue full benefits of this 2D layers based MOF for supercapacitor usage, a distinctive robust hybrid of **1** was mixed in an appropriate ratio with different 2D structured substance, i.e. rGO (**2**), by means of a ultra-sonication method (**Figure 1.13**). Prominent specific capacitance was revealed by electrochemical analyses of formed composite (**3**), along with remarkable cycling efficiency. [49]



Figure 1.12 A schematic representation of Na/Zn-MOF (1).

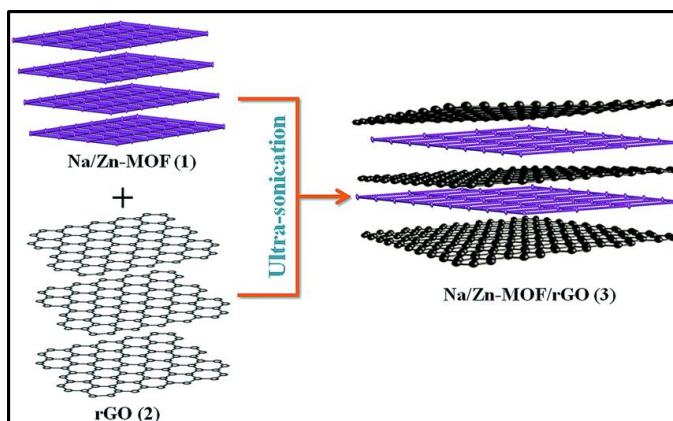


Figure 1.13 A plausible schematic diagram of the formation of 3.

1.5 Organization of the thesis

The purpose of this project was to design and synthesis of functional linker for the construction MOFs and their application in energy storage. This was to be achieved by hydrothermal process followed by cyclic voltammetry.

Chapter 2: In this chapter, we have discussed about the past and present works on the 2D MOFs for the energy storage application.

Chapter 3: This chapter includes materials, techniques and experimental procedure which were used to synthesize MOFs.

Chapter 4: In this chapter, we have discussed about the results that was obtained during synthesis of these compounds.

Chapter 5: In this chapter, we have concluded all the results of our work and their future aspects.

Chapter 2

Review of Past and Present Work

Metal-organic frameworks (MOFs) are inorganic-organic hybrid materials and represent a very important and exponentially rising chemical and material analysis field thanks to their structural skillfulness and utility for a large spectrum of applications together with gas surface assimilation, separation, and chemical process, sensing, optical and magnetic besides medical specialty functions. Precise coming up with ways, standardization of self-assembly method and development of efficient artificial protocols are the modern challenges of this field. Crystal engineering tools combining with innovative artificial approaches enable North American country to realize the really ‘tailored’ MOFs for desired applications. They typically exhibit some characteristic features: extremely regular channels, manageable pore size, giant internal area and designable pore surface practicality that play crucial roles in varied useful properties.

The Zn(II) ions are the foremost ordinarily reportable metals and show smart energy storage properties once coordinated by multidentate ligands. A major variety of MOFs containing Zn(II) ions with energy storage properties are ascertained. To date, Brobdingnag amounts of coordination assemblies with fascinating compositions and properties are ready employing a wide diversity of aromatic polycarboxylate- and pyridine-based ligands.

In the present work, a carboxylate based Synthesis of 5-(1-oxoisindolin-2-yl)isophthalic acid (**H₂L**) has been synthesized. By using this ligand we have synthesized two coordination polymer in presence of (E)-1,2-di(pyridine-4-yl)ethane (dpe) and (E)-1,2-di(pyridine-4-yl)diazene (azodpe) as a co-ligand with Zn(II) ions under hydrothermal condition. The CP with dpe is one dimensional while with azodpe it is two

dimensional. The 2D framework showed smart energy storage property in binary compound Na_2SO_4 and conjointly used as material for supercapacitor.

Chapter 3

Experimental section

3.1. Materials

All the reagents employed were commercially available and used as provided without further purification. $\text{Zn}(\text{NO}_3)_2 \cdot 6\text{H}_2\text{O}$ (98%), 5-Aminoisophthalic acid, and 2-(bromomethyl)benzonitrile were obtained from Sigma Aldrich and used as received. Other chemicals *i.e.* HCl, KOH, K_2CO_3 , SOCl_2 and solvents were procured from Loba Chemie and S. D. fine Chemicals (India). All solvents were dried and purified prior to use following standard methods.

3.2. Methods and instrumentation

Reactions were monitored by TLC on Merck silica gel plates and spot were viewed under UV lamp. Column chromatography was performed using silica gel or neutral alumina. ^1H NMR spectra and ^{13}C NMR were recorded on a JEOL JNM-LA 400 FT (400 and 80 MHz respectively) instrument in d_6 -DMSO with Me_4Si as the internal standard. The splitting patterns of ^1H NMR peaks are denoted as: s, singlet; d, doublet; t, triplet; q, quartet; m, multiplate. ESI-mass spectra were obtained by the WATERS Q-TOF Premier mass spectrometer.

3.3. Electrochemical measurements

The electrochemical studies were conceded on an electrochemical workstation (Autolab PGSTAT 204N). A three electrode standard configuration including counter electrode platinum wire, reference electrode Ag/AgCl and a 3 mm diameter glassy carbon electrode (GCE) as

the working electrode was assimilated. All dimensions and measurements were performed at room temperature (RT).

3.4. X-Ray crystallography

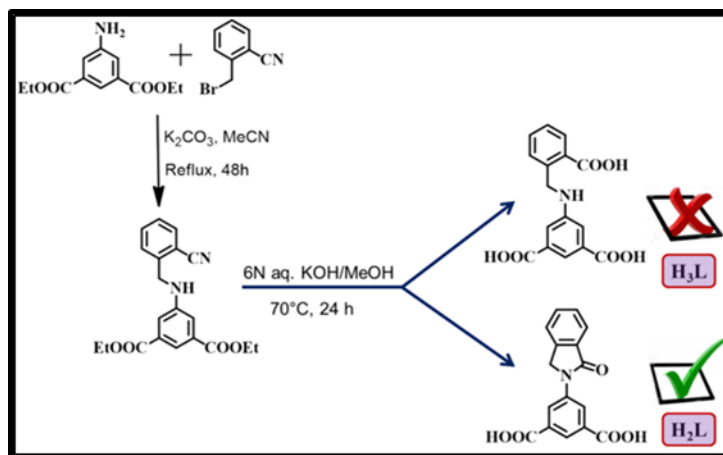
Single crystal X-ray data were collected at 100K, on a Bruker SMART APEX CCD diffractometer using graphite monochromated MoK α radiation ($\lambda = 0.71073\text{\AA}$) at IIT Kanpur. The linear absorption coefficients, scattering factors for the atoms, and the anomalous dispersion corrections were taken from International Tables for X-ray Crystallography. The data integration and reduction were processed with SAINT software. An empirical absorption correction was applied to the collected reflections with SADABS using XPREP. The structure was solved by the direct method using SHELXTL and refined on F^2 by full-matrix least-squares technique using the SHELXL-97 program package. All non-hydrogen atoms were refined anisotropically. All hydrogen atoms were located in successive difference Fourier maps and they were treated as riding atoms using SHELXL default parameters.

3.5. Synthesis of organic Linkers

We have synthesized a previously reported dicarboxylic acid based linker with the secondary functional groups, described below.

3.5.1. Synthesis of H₂L

The ligand H₂L was synthesized in several steps as shown in **scheme 1**.



Scheme 1. The synthetic scheme for preparation of **H₂L**.

3.5.1.1. Synthesis of diethyl 5-((2-cyanobenzyl) amino)isophthalate

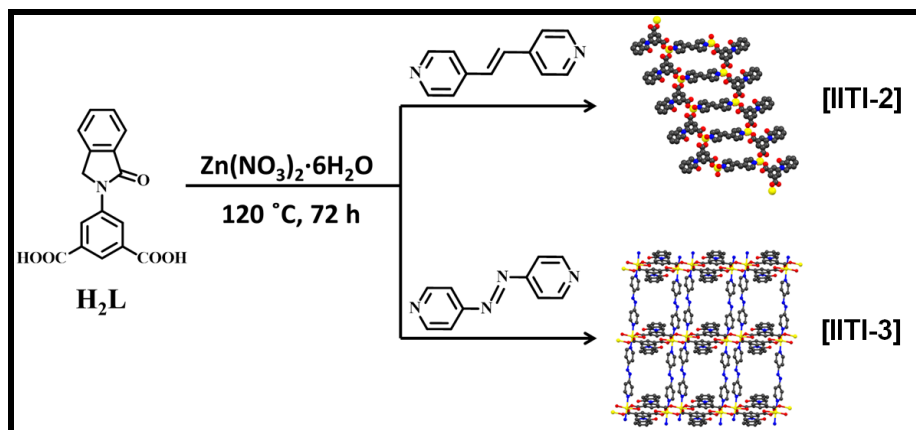
In an N₂ atmosphere, diethyl-5-aminoisophthalate (2 g, 8.4 mmol) was taken in a round-bottom flask and added dry acetonitrile (100 mL) and followed by mixing of dry K₂CO₃ (1.6 g, 12.3 mmol) in a round-bottom flask maintaining an inert atmosphere, and the mixture was stirred for 30 min at 80 °C. The mixture was treated with 2-(bromomethyl)benzonitrile (1.65 g, 8.4 mmol), after with the solution undergo reflux for 24 h. At the end, solution was cooled to room temperature and poured in ice-cold water (70 mL), then white solid was collected by filtration method and air dried. Yield: 2.7g (91%). ¹H-NMR (CDCl₃, 400 MHz, 25 °C, Me₄Si): δ = 8.8003(s, 2H, Ar-H), 8.4001 (s, 1H, N-H), 7.6911 (d, 1H, J = 6.88 Hz, Ar-H), 7.5380 - 7.4605 (m, 4H, Ar-H), 4.9692 (s, 2H), 4.4153 (q, 4H, J = 7.18 Hz, -CH₂-), 1.4148 (t, 6H, J = 7.16 Hz, -CH₃) ppm (**Figure 4.1**); ¹³C NMR (CDCl₃, 100 MHz, 25 °C, Me₄Si): δ = 165.97, 150.92, 145.77, 138.05, 131.81, 131.32, 128.28, 124.71, 124.43, 122.95, 121.73, 101.83, 61.58, 53.46, 14.44 ppm (**Figure 4.2**); ESI-MS: m/z [M+H]⁺ 353.15 (100%)(**Figure 4.3**).

3.5.1.2. Synthesis of 5-(1-oxoisindolin-2-yl)isophthalic acid (H₂L)

Above obtained compound (2 g, 5.17 mmol) was hydrolyzed with 6(N) NaOH solution (20 mL) for 24 h in reflux conditions. After cooling to 5 °C, the acidification of the resulting solution was carried out with 6(N) HCl solution to acquire a white precipitate which was filtrated, washed with water many times, and dried in air. Yield: 1.35 g (80%). It has been characterized by ¹H, ¹³C NMR, mass Spectrometry, elemental analysis. ¹H NMR (*d*₆-DMSO, 400 MHz, 25 °C, Me₄Si): δ = 8.6766 (s, 2H, Ar-H), 8.2290 (s, 1H, -NH), 7.7869 – 7.7679 (d, 1H, J = 7.60Hz, Ar-H), 7.6720 – 7.6572 (m, 2H, Ar-H), 7.5433 – 7.5037 (m, 1H, Ar-H), 5.1083 (s, 2H, -CH₂-) ppm (**Figure 4.4**); ¹³C NMR (DMSO-*d*₆, 100 MHz, 25 °C, Me₄Si): δ = 167.64, 167.05, 141.68, 140.66, 133.01, 132.66, 132.50, 128.83, 125.60, 124.04, 123.94, 123.69, 50.97 ppm (**Figure 4.5**); ESI-MS: *m/z* [M]⁺ 298.07 (100) (**Figure 4.6**).

3.5.2. Synthesis of CP/MOF

The ligand H₂L was synthesized in several steps as shown in **Scheme 2**.



Scheme 2. The synthetic scheme for preparation of IITI-2 and IITI-3.

3.5.2.1. Synthesis of **IITI-2**

H₂L (15 mg, 0.6 mmol), Zn(NO₃)₂·6H₂O (60 mg, 0.20 mmol), (E)-1,2-di(pyridine-4-yl)ethane (dpe) (15 mg, 0.6 mmol) and NaOH (1 M, 20 μL) were dissolved with water (3 ml H₂O) in a 5 mL Teflon vessel and heated for 72 h at 120 °C. After cooling the above set up to room temperature, the resulting light pink color needle-shaped crystals (**IITI-2**) were collected and washed repeatedly with H₂O and acetone and dried in air to obtain a high yield of 83% (based on the ligand).

3.5.2.2. Synthesis of **IITI-3**

H₂L (15 mg, 0.6 mmol), Zn(NO₃)₂·6H₂O (60 mg, 0.20 mmol), (E)-1,2-di(pyridine-4-yl)diazene (azodpe) (15 mg, 0.6 mmol) and NaOH (1 M, 20 μL) were dissolved with water (3 mL) in a 5 mL Teflon vessel and heated for 72 h at 120 °C. After cooling the whole set up to room temperature, the resulting light pink color needle-shaped crystals (**IITI-3**) were collected and washed four to five times with H₂O, followed by acetone and dried in air to give a high yield of 83% (based on the ligand).

Chapter 4

Result and discussion

IIT-2 and **IIT-3** are synthesized by the hydrothermal reaction of $\text{Zn}(\text{NO}_3)_2 \cdot 6\text{H}_2\text{O}$ and H_2L with dpe and azodpe as co-linkers in H_2O in alkaline medium at 120 °C. The presence of bidentate ligand and tendency of Zn to form MOFs have led for the formation of these two unreported MOFs. The linker H_2L was characterized by mass spectrometry and NMR spectroscopy. The CP and MOF were characterized by single crystal X-ray diffraction (SC-XRD) studies.

4.1. Characterization of diethyl 5-((2-cyanobenzyl) amino)isophthalate

4.1.1. NMR Spectroscopy

NMR spectrum of diethyl 5-((2-cyanobenzyl) amino)isophthalate were recorded in CDCl_3 using TMS as an internal standard. In ^1H NMR aromatic proton peaks were observed at about 8.803 ppm, 7.6911 ppm, 7.5380-7.4605 ppm, at 8.4001 corresponds to NH proton, peak at 4.92692 ppm, 4.4153 ppm and 1.4148 ppm correspond to CH_2 of NH, CH_2 of ethyl and CH_3 of ethyl proton (**Figure 4.1**). In ^{13}C NMR spectrum of 5-((2-cyanobenzyl) amino)isophthalate aromatic carbon peaks were shown at 121-150 ppm, 14.44 ppm corresponds to CH_3 of ester, 53.46 ppm corresponds to CH_2 of ester, 61.58 ppm corresponds to CH_2 near to amine, 101.81 ppm corresponds to CN and COO carbon peaks shown at 165.97 ppm (**Figure 4.2**).

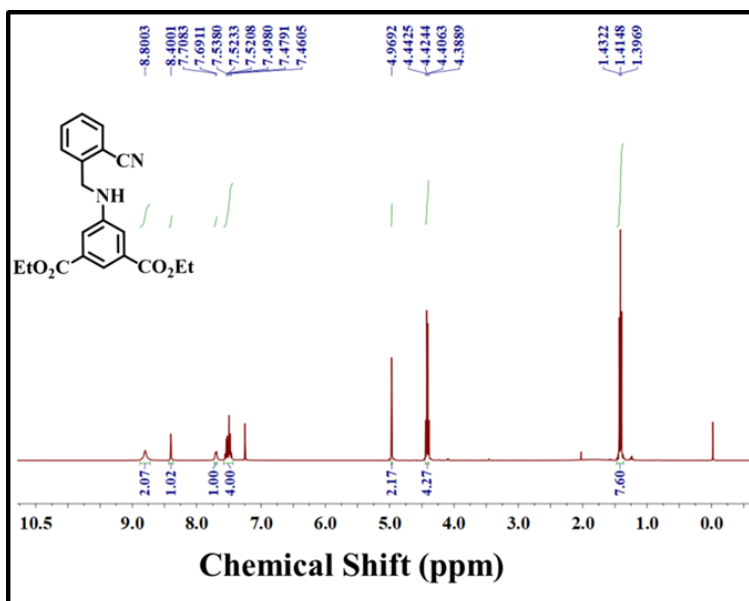


Figure 4.1 The ^1H NMR spectrum of diethyl 5-(2-cyanobenzoyloxy)isophthalate.

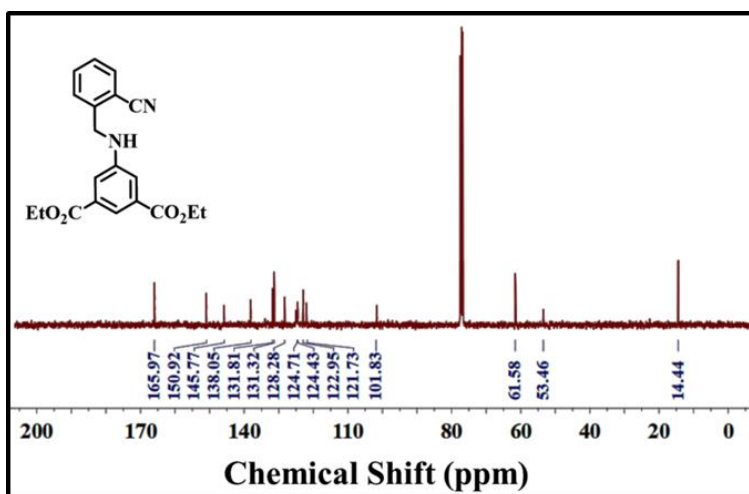


Figure 4.2 The ^{13}C NMR spectrum of diethyl 5-(2-cyanobenzoyloxy)isophthalate

4.1.2. Mass Spectrometry

ESI-MS data supports the formation of diethyl 5-((2-cyanobenzyl) amino)isophthalate with molecular ion peak at m/z 353.15 (100%) which corresponds to $[\text{M}+\text{H}]^+$ (Figure 4.3).

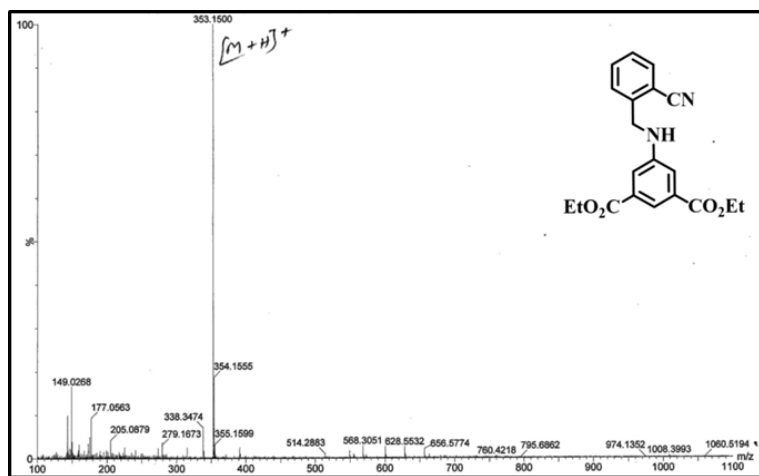


Figure 4.3 ESI-MS spectrum of diethyl 5-((2-cyanobenzyl) amino)isophthalate.

4.2. Characterization of H₂L

4.2.1. NMR Spectroscopy

NMR spectra of H₂L were recorded in *d*₆-DMSO using TMS as an internal standard. In ¹H NMR 5.11 corresponds to the CH₂ group of the amine, 8.68 ppm peak corresponds to the two proton present near to carboxylic group, 8.23 ppm corresponds to the proton present between the two carboxylic group, 7.79 ppm corresponds to the proton present near ortho to the carbonyl group, 7.50 ppm corresponds to the meta to the carbonyl group and rest of the two aromatic proton corresponds to the 7.67 ppm respectively (**Figure 4.4**). ¹³C NMR spectrum of H₂L shows 50.97 ppm corresponds to the CH₂ carbon, 167.05 ppm corresponds to the CO carbon, 167.64 ppm corresponds to the COO carbon and other signals are for aromatic region (**Figure 4.5**).

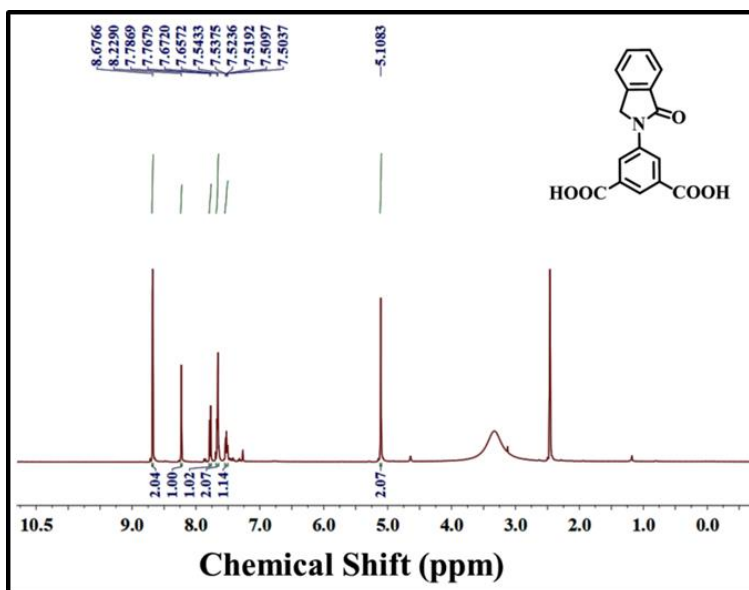


Figure 4.4 The 1H NMR spectrum of H_2L .

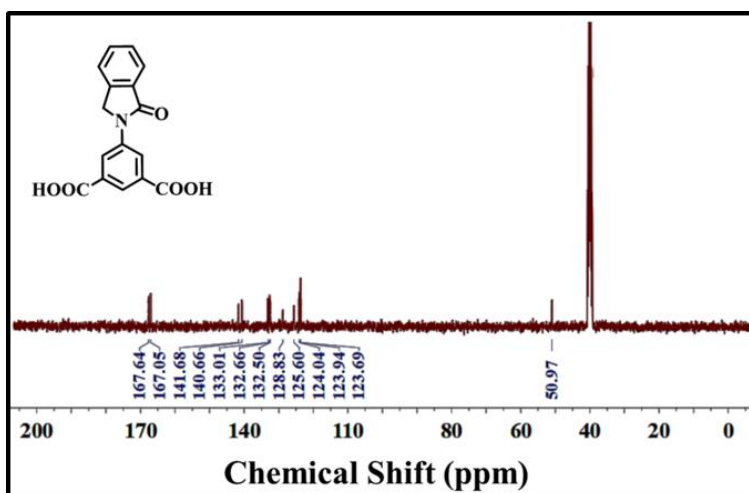


Figure 4.5 The ^{13}C NMR spectrum of H_2L .

4.2.2. Mass spectrometry

EI-MS data supports the formation of L1 with molecular ion peak at m/z is 298.07 (100)183 which corresponds to $[M+H]^+$ (Figure 4.6).

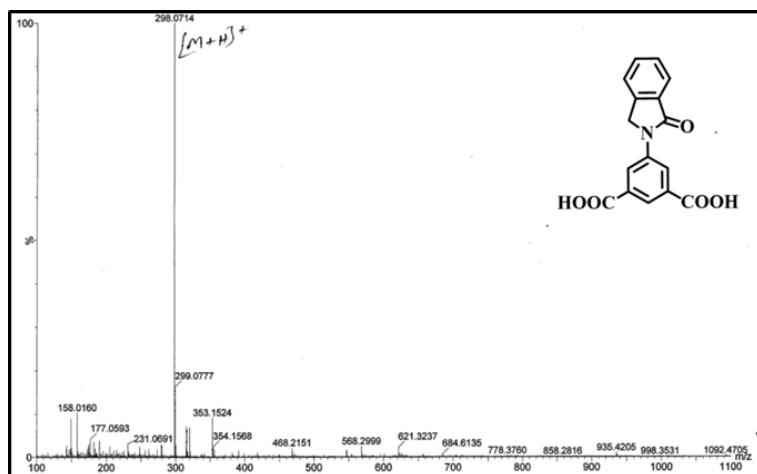


Figure 4.6 ESI-MS spectrum of H_2L .

4.3. Crystal structure of IIT-2

SC-XRD studies reveal that Zn-dpe (**IIT-2**) crystallizes in a monoclinic system with the $P2_1/c$ space group. **Figure 4.7(a)** displays the asymmetric unit of **IIT-2**, which contains one Zn(II) ion, one (H_2L) unit, half dpe molecule, one H_2O molecule and two free H_2O molecules. **Figure 4.7(b)** exhibits the coordination of each Zn(II) ion with two O atoms of two different H_2L molecules, one H_2O molecule at axial position and one N atom of dpe linker at equatorial positions. Each Zn(II) ion is in an O3N surroundings and organized with the formation of distorted tetrahedral geometry. The calculated bond distances for Zn–O vary from 1.902 to 2.040 Å, and the Zn–N distance is 2.019 Å. Additionally, two adjacent Zn(II) ions are 9.579 Å apart in one molecule (**Figure 4.7(c)**) which coordinates further forming a 1 D chain of ladder pattern along a -axis (**Figure 4.7(a)**). Additionally C–H \cdots O type hydrogen bond interactions between O004 of one molecule and H00B of adjacent molecules exist in **IIT-2** with the distance O00U5–H00B \cdots O004 = 1.805 Å and $\angle\text{C14–H14}\cdots\text{O} = 171.67^\circ$ forming a 2D framework along b -axis (**Figure 4.8(b)**).

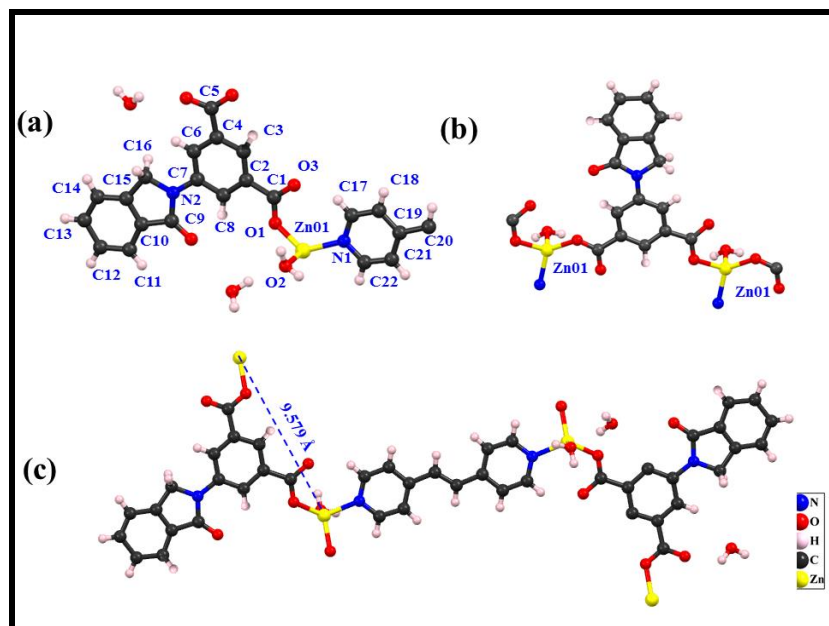


Figure 4.7 (a) Asymmetric unit of **IITI-2**, (b) Coordination environment around Zinc ions and (c) perspective view of **IITI-2**.

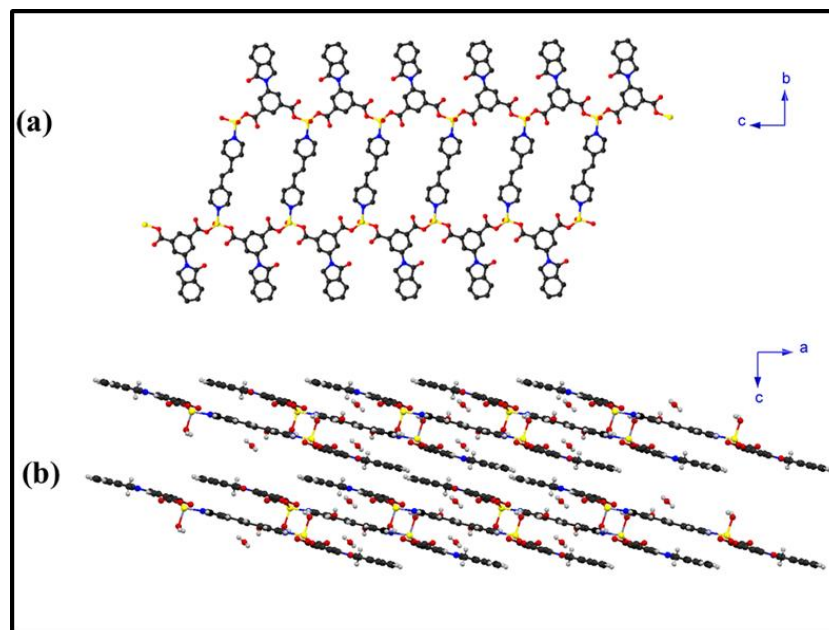


Figure 4.8 (a) 1-D framework of **IITI-2**, (b) 2-D framework of **IIT-2** formed by hydrogen bonding interactions.

4.4. Crystal structure of **IITI-3**

SC-XRD studies reveal that Zn-azodpe 2D (**IITI-3**) crystallizes in a triclinic system with the *P*-1 space group. **Figure 4.9(a)** displays the

asymmetric entity of **IIIT-3**, which consists of one Zn(II) ion, one (H₂L) unit and one azodpe molecule. **Figure 4.9(b)** displays the coordination of each Zn(II) ion with four O atoms of three different H₂L molecules at equatorial positions, two N atom of two azo-dpe linker at axial positions.

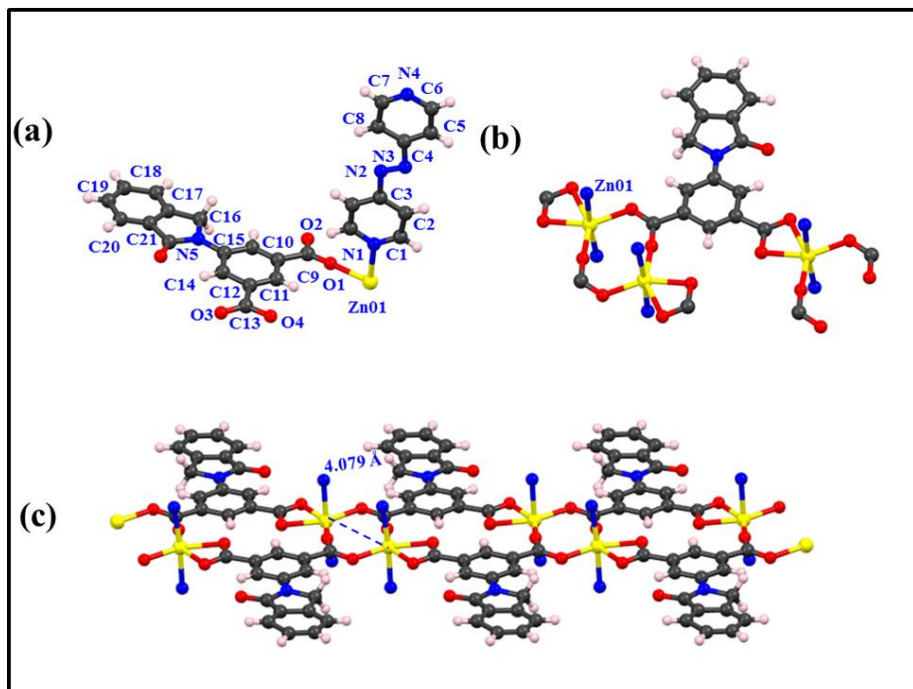


Figure 4.9 (a) Asymmetric unit of **IIIT-3**, (b) Coordination environment around Zinc ions and (c) 1-D chain of **IIIT-3**.

Each Zn(II) ion is present in an O₄N₂ surroundings and organized with distorted square planar bi-pyramidal geometry with the formation of 1-D layers **Figure 4.9(c)**. The bond distances observed in the crystal structure for Zn–O range from 2.028 to 2.323 Å, while the Zn–N distances are 2.188 Å and 2.143 Å. Additionally, two Zn(II) ions are at a distance of 4.079 Å in each cluster. The obtained 1D layers are further pillared by azo-dpe molecule developing a 2D framework having square rings along the *c*-axis **Figure 4.9(a)**. The 1D chain are 13.344 Å distance apart through azo-dpe linkers (**Figure 4.10(a)**). Additionally C–H···O type hydrogen bond interactions between O001 of one molecule and H00A of adjacent molecules exist in 1 with the distance C00U–H00A···O001 =

2.642 Å and $\angle\text{C14-H14}\cdots\text{O} = 129.79^\circ$ forming a self-assembled 3D framework (**Figure 4.10(b)**).

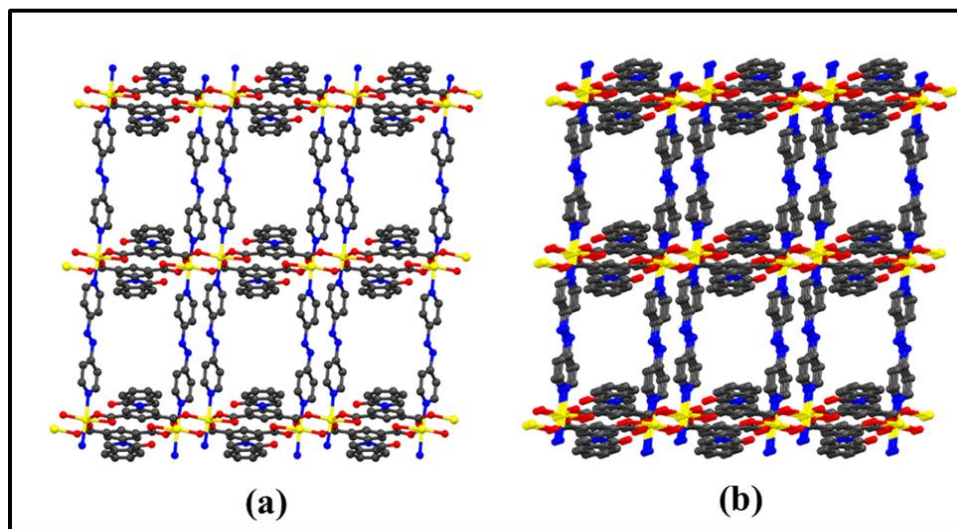


Figure 4.10 (a) View of 2-D framework of **IITI-3**, (b) 3-D framework of **IITI-3** through hydrogen bonding interactions.

4.5. Electrochemical energy storage application of **IITI-3**

A 3-electrode cell was utilized to carry out the electro-chemical measurements of **IITI-3** using in 1 M Na_2SO_4 aqueous electrolyte without using any profitable files. This tactic of homework of file less employed electrode is profitable for everyday device properties. The drop-cast fabricated rodes of **IITI-3** are denoted as **IITI-3/GCE**, and their properties for super capacitors were likened methodically by Galvanostatic charge–discharge (GCD) and cyclic voltammetry (CV) methodes.

In the primarily accompanied experiments, the electrode CV profiles was related at 100 mV s^{-1} , which displays a slightly improved charge transmission and combined region under the curve for **IITI-3/GCE**. This observation recommends some amount of specific capacitance of **IITI-3**.

The CV outlines of **IITI-3/GCE** displays a somewhat enough charge transference having an improved induced current when compared to bare electrode (**Figure 4.11**). Furthermore, CV curves at altered scan

rates (25-500 mV s^{-1}) denotes non ideal shape in voltammogram, which propose the nonexistence of double layer capacitive progression and presence of peaks acclaims the probability of pseudo capacitive route

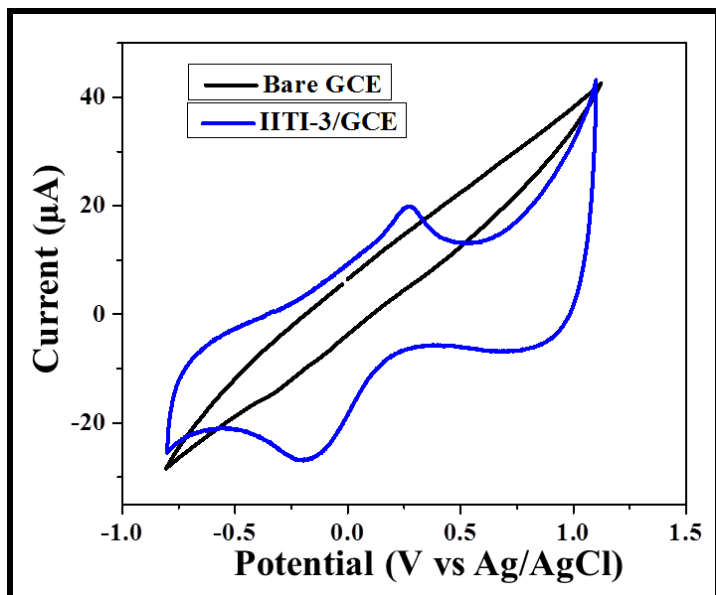


Figure 4.11 Comparisons of the CV profiles of bare GCE and IITI-3/GCE at scan rate of 100 mV s^{-1} .

having good charge transmission compared to bare electrode. Though, it is unsatisfactory to produce in elevated specific capacitance. The improved form of current response of IITI-3/GCE can be considered by comparing the y-axes of **Figure 4.12**. Observing the CV curves in profile, it is perceived that IITI-3/GCE exhibit stimulated charge transmission and storage capability. The constantly upgraded CV integrated area underneath the CV curves for IITI-3/GCE beside the improved current response devoid of any visible signal damage at greater scan rates, disclose decent charge storage features and elevated rate ability. This amplified charge storage and linked properties is the result of the expanded MOF construction of 2D Zn-MOF. In conclusion, the encouraged charge stocking features in IITI-3/GCE can be allocated for a pseudo capacitive IITI-3/GCE.

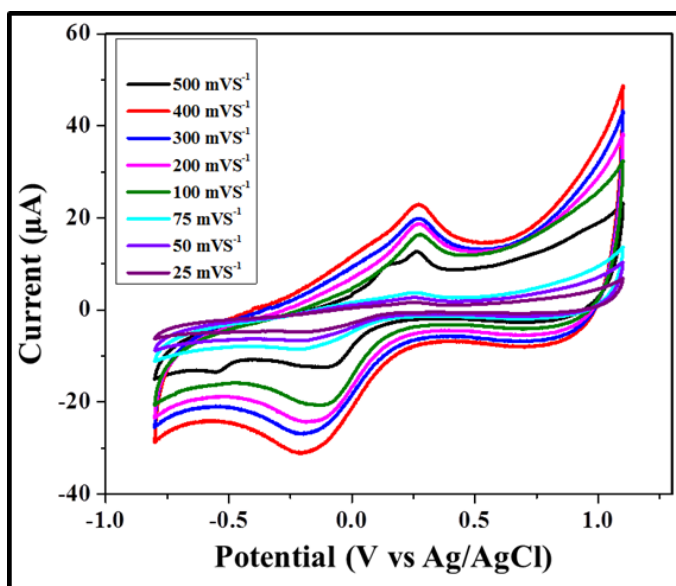


Figure 4.12 CV profiles of IITI-3/GCE at different scan rates (10-500 mV s⁻¹)

The assessment of GCD curves is presented in **Figure 4.13**, which displays some amount of time to discharge in case of IITI-3/GCE. This consideration advises some amount of specific capacitance of IITI-3/GCE over bare electrode. IITI-3/GCE shows a disturbed triangular outline of GCD graphs owing to probable supremacy of oxidation-reduction procedure, this shows that the presence pseudo capacitance (**Figure 4.11**). Though, there is not at all potential drop seemed in IITI-3/GCE at all scan rates and current densities which specifies the least inner resistance, which expresses its dressed charge storage ability and conductivity. The GCD graph outlines at separately current density spectacles the good discharge time for IITI-3/GCE over bare electrode, which is the approval of certain specific capacitance. These outcomes are in mark with those attained concluded CV. The experimental specific capacitances for IITI-3/GCE at current densities of 0.48, 056, 0.64, 0.72, 0.8, 0.88 and 0.96 are 7.2, 8.4, 8.8, 10.8, 9.5, 9.35 and 8.76 F g⁻¹, correspondingly. After doing all calculations, areal capacitance at 0.127 mA cm⁻² was 0.067 Fcm⁻².

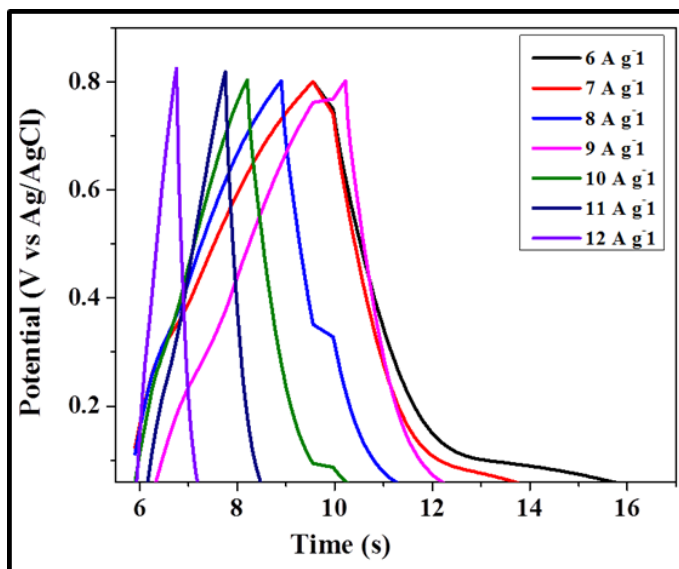


Figure 4.13 GCD profiles of IITI-3/GCE at different current densities (6-12 A g⁻¹). (Electrolyte: 1M Na₂SO₄).

Table 1. A comparison of the supercapacitor performance of **IITl-3** with the previous state-of-the-art MOFs materials.

MOFs	Type of MOF	Synthetic conditions	Electrolyte	Specific Capacitance (F g ⁻¹)	Scan Rate (A g ⁻¹)	Ref.
Zn MOFs	Polycatenated	120 °C	1 M Li ₂ SO ₄	23	0.0025	50
Cd MOFs	Polycatenated	120 °C	1 M Li ₂ SO ₄	22	0.0025	50
In-MOF	Channel-type mesoporous	120 °C	6 M KOH	150.2	0.2	51
ZIF-67	Sodalite-type structure	RT stirring	1 M KOH	188.7	1	52
Co-MOF	Leaflet like structure	100 °C	0.5 M LiOH	131.8	10	53
Co8-MOF-5	Rectangular	105 °C		0.30	0.01	54
Cu-MOF	Blocked	Slow diffusion	1 M Na ₂ SO ₄	85	1.6	47
Ce-MOF	Blocked	Slow diffusion	3M KOH	94.8	1	55
Cu-MOF	Blocked	110 °C	0.5 M Na ₂ SO ₄	<50	4	56
Zn MOF (IITl-3)	Needle shaped	120 °C	1 M Na₂SO₄	10.8	0.9	This work

Chapter 5

Conclusion and Future Scope

In this thesis, a ligand 5-(1-oxoisindolin-2-yl)isophthalic acid (H_2L) was synthesized by substitution reaction between diethyl-5-aminoisophthalate and 2-(bromomethyl)benzotrile. Their molecular structure was confirmed by mass spectrometry and NMR spectroscopy.

Two new CP/MOF (**IITI-2** and **IITI-3**), were synthesized utilizing Zn(II) metal ions with H_2L and dpe/azodpe as co-linkers respectively. The structural study shows that the **IITI-2** is a 1D coordination polymer while **IITI-3** is a 2D metal-organic framework. The notable thing in this case of Zn(II) coordination polymer and metal-organic framework were, when reaction was carried in the presence of dpe at 120 °C the 1D coordination polymer was formed whereas the same reaction was carried in the presence of azodpe the 2D metal-organic framework formed i.e. the reaction is co-linker dependent because if we change the co-linker product will also change. It was observed that Zn(II) metal ions in the **IITI-2** formed distorted tetrahedral geometry while in **IITI-3** it formed distorted octahedral geometry. In **IITI-2**, two adjacent Zn(II) ions are separated by 9.579 Å in one molecule which further coordinates to create a 1 D chain of ladder pattern along *a*-axis and Additionally C–H···O type hydrogen bond interactions forming a 2D network along *b*-axis, while in case of **IITI-3**, two adjacent Zn(II) ions forming a metallacycle ring where both the Zn(II) ions are separated by 4.079 Å which extended to create a 1D layers which are pillared by azo-dpe molecule forming a 2D framework containing square shaped voids along the *c*-axis. Additionally C–H···O type hydrogen bond interactions forming a self-assembled 3D network. We were further investigated the electrochemical energy storage application of **IITI-3**

which gave comparable result in supercapacitor activity compared to other MOF based electrode materials.

Zn(II) based MOFs are very good candidates for the sensing applications viz. bio sensing, bio imaging, highly selective detection of nitro aromatic explosives, small molecules etc. Also, Zn-MOFs are utilized for the high performance lithium–sulfur battery.

In general 2D Zn-MOFs are interesting candidates for the fabrication of energy storage devices in supercapacitor and also the catalytic behavior of Zn(II) in biological systems are very interesting area of research in future.

APPENDIX-A

Table A1. Crystal structure and refinement parameters for **IITI-2** and **IITI-3**.

Parameters	IITI-2	IITI-3
Empirical formula	C ₂₂ H ₂₀ N ₂ O ₈ Zn	C ₂₆ H ₁₇ N ₅ O ₅ Zn
Formula wt.	505.74	544.82
Crystal system	Monoclinic	Triclinic
Space group	<i>P</i> 2 ₁ / <i>c</i>	<i>P</i> -1
<i>a</i> , Å	10.3165(8)	10.0192(9)
<i>b</i> , Å	9.5620(8)	13.3441(15)
<i>c</i> , Å	22.6902(15)	14.680(2)
α (deg)	90	100.841(10)
β (deg)	94.527(7)	100.374(9)
γ (deg)	90	92.200(8)
<i>V</i> , Å ³	2231.3(3)	1890.9(4)
<i>Z</i>	4	2
ρ_{calc} g/cm ³	1.497	0.957
μ , mm ⁻¹	1.515	0.680
Temperature (K)	293	293
θ max	29.087	17.3640
F(000)	1028	556
Refl. Collected	26061	18827
Independent refl.	5459	8843
GOOF	0.957	0.886
Final R indices (R_1^a , wR_2^b) [$I > 2\sigma(I)$]	10.95, 22.08	9.97, 23.70
R indices (R_1^a , wR_2^b) (all data)	31.81, 31.35	22.33, 29.36

$$^a R_1 = \sum(|F_o| - |F_c|) / \sum |F_o|. \quad ^b R_2 = [\sum\{w(F_o^2 - F_c^2)^2\} / \sum\{w(F_o^2)^2\}]^{1/2}.$$

Table A2. Selected bond distances (Å) and bond angles (°) in **III-2**.

[Zn(L)(dpe) _{0.5} (H ₂ O)]·2H ₂ O (III-2)			
Bond distances (Å)			
Zn01–O002	1.901(6)	Zn01 – O003	1.930(7)
Zn01 – O005	2.041(6)	Zn01 – N006	2.018(7)
C00O – C00O	1.338(18)		
Bond angles (°)			
O002–Zn01–O003	117.9(3)	O002–Zn01–O005	105.7(3)
O002–Zn01–N006	125.5(3)	O003–Zn01–O005	104.2(3)
O003–Zn01–N006	101.6(3)	N006–Zn01–O005	98.6(3)
C00A–O002–Zn01	123.2(6)	C00R–O003–Zn01	120.6(7)
C00F–N006–Zn01	124.7(6)	C00G–N006–Zn01	118.9(6)

Table A3. Selected bond distances (Å) and bond angles (°) in **III-3**.

[Zn(L)(azodpe)]·(Solvent) _x (III-3)			
Bond distances (Å)			
Zn01 – O002	2.028(5)	Zn01 – O003	2.050(7)
Zn01 – O004	2.323(6)	Zn01 – O005	2.138(6)
Zn01 – N006	2.188(7)	Zn01 – N007	2.143(7)
N00E – N00M	1.160(10)		
Bond angles (°)			
O002–Zn01–O003	119.9(2)	O002–Zn01–O004	89.1(2)
O002–Zn01–O005	148.3(3)	O002–Zn01–N006	88.7(3)
O002–Zn01–N007	88.0(2)	O002–Zn01–C00H	118.1(3)
O003–Zn01–O004	151.0(2)	O003–Zn01–O005	91.9(3)
O003–Zn01–N006	88.0(3)	O003–Zn01–N007	90.2(3)
O003–Zn01–C00H	122.0(3)	O004–Zn01–C00H	29.0(3)
O005–Zn01–O004	59.2(2)	O005–Zn01–N006	92.9(2)
O005–Zn01–N007	92.0(2)	O005–Zn01–C00H	30.2(3)
N006–Zn01–O004	91.0(2)	N006–Zn01–C00H	91.2(3)
N007–Zn01–O004	92.9(2)	N007–Zn01–N006	174.8(2)
N007–Zn01–C00H	93.9(3)	C009–O002–Zn01	120.5(6)
C009–O003–Zn01	172.2(6)	C00H–O004–Zn01	86.2(5)
C00H–O005–Zn01	93.3(6)	C00J–N006–Zn01	122.5(7)
C00K–N006–Zn01	118.7(7)		

References

- [1]. Batten S.R., Baquet G., Champness N.R., Chen X.M., Martinez J.C., Kitagawa S., Oehstroem L., O’Keeffe L., Suh M.P., Reedjik J. (2012), Coordination polymers, Metal-organic frameworks and need for terminology guidelines, *Cryst Eng Comm*, 14,3001-3004 (DOI: 10.1039/c2ce06488j)
- [2]. Sen S.K., Natarajan R. (2019), Influence of Conformational Change and Interligand Hydrogen Bonding in a Chiral Metal–Organic Cage, *Inorg Chem*, 58, 11, 7180-7188 (DOI: 10.1021/acs.inorgchem.8b03610)
- [3]. Duan J., Li Y., Pan Y., Behera N., Jin W. (2019), Metal-organic framework nanosheets: An emerging family of multifunctional 2D materials, *Coordination Chemistry Reviews*, 395, 25-45 (DOI: 10.1016/j.ccr.2019.05.018)
- [4]. Wang Y.Y., Liu Y.C., Sun H., Guo D.S. (2019), Type I photodynamic therapy by organic–inorganic hybrid materials: From strategies to applications, *Coordination Chemistry Review*, 395, 46-62 (DOI: 10.1016/j.ccr.2019.05.016)
- [5]. Tchalala M.R., Bhatt P.M., Chappanda K.N., S. R. Tavares, Adil K., Belmabkhout Y., Shkurenko A., Cadiau A., Heymans N., Weireld G.D., Maurin G., Salama K.N., Eddaoudi M. (2019), Fluorinated MOF platform for selective removal and sensing of SO₂ from flue gas and air, *Nature Communications*, 10, 1328 (DOI: 10.1038/s41467-019-09157-2)
- [6]. Li Y.J., Wang Y.L., Liu Q.Y. (2017), The Highly Connected MOFs Constructed from Nonanuclear and Trinuclear Lanthanide-Carboxylate Clusters: Selective Gas Adsorption and Luminescent pH Sensing, *Inorg Chem*, 56, 4, 2159-2164 (DOI: 10.1021/acs.inorgchem.6b02811)

- [7]. Chen B., Ma S., Hurtado E.J., Lobkovsky E.B., Liang C., Zhu H., Dai S. (2007), Selective Gas Sorption within a Dynamic Metal-Organic Framework, *Inorg Chem*, 46, 21, 8705-8709 (DOI: 10.1021/ic7013573)
- [8]. Zhao N., Sun F., Li P., Mu X., Zhu G. (2017), An Amino-Coordinated Metal–Organic Framework for Selective Gas Adsorption, *Inorg Chem*, 56, 12, 6938-6942 (DOI: 10.1021/acs.inorgchem.7b00436)
- [9]. Koizumi K., Nobusadaab K., Boeroc M. (2019), Hydrogen storage mechanism and diffusion in metal–organic frameworks, *Phys Chem Chem Phys*, 21, 7756-7764 (DOI: 10.1039/C8CP07467D)
- [10]. Kang Z., Fan L., Sun D. (2017), Recent advances and challenges of metal–organic framework membranes for gas separation, *J Mater Chem A*, 5, 10051-10724 (DOI: 10.1039/C7TA01142C)
- [11]. Kapelewski M.T., Runcevski T., Tarver J.D., Jiang Z.H.H., Hurst K.H., Parilla P.A., Ayala A., Gennett T., FitzGerald S.A., Brown C.M., Long J.R. (2018), Record High Hydrogen Storage Capacity in the Metal–Organic Framework Ni₂(m-dobdc) at Near-Ambient Temperatures, *Chem Mater*, 30, 22, 8179-8189 (DOI: 10.1021/acs.chemmater.8b03276)
- [12]. Li H., Wang K., Sun Y., Lollar C.T., Li J., Zhou H.C. (2018), Recent advances in gas storage and separation using metal–organic frameworks, *Materials Today*, 21, 2, 108-121 (DOI: 10.1016/j.mattod.2017.07.006)
- [13]. Wang D., Gates B.C. (2019), Catalysis by Metal Organic Frameworks: Perspective and Suggestions for Future Research, *ACS Catal*, 9, 3, 1779-1798 (DOI: 10.1021/acscatal.8b04515)
- [14]. Wang C., An B., Lin W. (2019), Metal–Organic Frameworks in Solid–Gas Phase Catalysis, *ACS Catal*, 9, 1, 130-146 (DOI: 10.1021/acscatal.8b04055)

- [15]. Dhakshinamoorthy A., Li Z., Garcia H. (2018), Catalysis and photocatalysis by metal organic frameworks, *Chem Soc Rev*, 47, 8134-8172 (DOI: 10.1039/C8CS00256H)
- [16]. Zhang H., Liu X., Wu Y., Guan C., Cheetham A.K., Wang J. (2018), MOF-derived nanohybrids for electrocatalysis and energy storage: current status and perspectives, *Chem Commun*, 54, 5268-5288 (DOI: 10.1039/C8CC00789F)
- [17]. Diamantis S.A., Margariti A., Pournara A.D., Papaefstathiou G.S., Manos M.J., Lazarides T. (2018), Luminescent metal–organic frameworks as chemical sensors: common pitfalls and proposed best practices, *Inorg Chem Front*, 8, 5, 1493-1511 (DOI: 10.1039/C8QI00090E)
- [18]. Zhang Q., Wang C.F., Lv Y.K. (2018), Luminescent switch sensors for the detection of biomolecules based on metal–organic frameworks, *Analyst*, 143, 4221-4229 (DOI: 10.1039/C8AN00816G)
- [19]. Fang S., Zong B., Mau S. (2018), Metal–Organic Framework-Based Sensors for Environmental Contaminant Sensing, *Nano-Micro Lett*, 10:64 (DOI: 10.1007/s40820-018-0218-0)
- [20]. Zhou Y., Li C., Hao Y., Ye B., Xu M. (2018), Oriented growth of cross-linked metal-organic framework film on graphene surface for non-enzymatic electrochemical sensor of hydrogen peroxide in disinfectant, *Talanta*, 188, 282-287 (DOI: 10.1016/j.talanta.2018.05.078)
- [21]. Aulakh D., Liu L., Varghese J.R., Xie H., Islamoglu T., Duell K., Kung C., Hsiung C., Zhang Y., Drout R.J., Farha O.K., Dunbar K.R., Han Y., Wriedt M. (2019), Direct Imaging of Isolated Single-Molecule Magnets in Metal–Organic Frameworks, *J Am Chem Soc*, 141, 7, 2997-3005 (DOI: 10.1021/jacs.8b11374)
- [22]. Huang L., Cai J., He M., Chen B., Hu B. (2019), Room-Temperature Synthesis of Magnetic Metal–Organic Frameworks Composites in Water for Efficient Removal of Methylene Blue and

- As(V), *Ind Eng Chem Res*, 57,18, 6201-6209 (DOI: 10.1021/acs.iecr.7b05294)
- [23]. Hu P., Yin L., Kirchon A., Li J., Li B., Wang Z., Ouyang Z., Zhang T., Zhou H. (2018), Magnetic Metal–Organic Framework Exhibiting Quick and Selective Solvatochromic Behavior along with Reversible Crystal-to-Amorphous-to-Crystal Transformation, *Inorg Chem*, 57, 12, 7006-7014 (DOI: 10.1021/acs.inorgchem.8b00703)
- [24]. Meng H., Zhao C., Nie M., Wang C., Wang T. (2018), Optically Controlled Molecular Metallofullerene Magnetism via an Azobenzene-Functionalized Metal–Organic Framework, *ACS Appl Mater Interfaces*, 10, 38, 32607-32612 (DOI: 10.1021/acsami.8b11098)
- [25]. Kukkar D., Vellingiri K., Kim K., Deep K. (2018), Recent progress in biological and chemical sensing by luminescent metal-organic frameworks, *Sensors and Actuators B: Chemical*, 237, 10, 1346-1370 (DOI: 10.1016/j.snb.2018.06.128)
- [26]. Allendorf M.D., Bauer C.A, Bhaktaa R.K., Houka R. J. T. (2009), Luminescent metal–organic frameworks, *Critical Review*, 38, 1330-1352 (DOI: 10.1039/B802352M)
- [27]. Xing X., Fu Z., Zhang N., Yu X., Wang M., Gou G. (2019), High proton conduction in an excellent water-stable gadolinium metal–organic framework, *Chem Commun*, 55, 1241-1244 (DOI: 10.1039/C8CC08700H)
- [28]. Bhardwaj S.K., Bhardwaj N., Kaur R., Mehta J., Sharma A.L., Kim, H.K., Deep A. (2018), An overview of different strategies to introduce conductivity in metal–organic frameworks and miscellaneous applications thereof, *J Mater Chem A*, 6, 14992-15009 (DOI: 10.1039/C8TA04220A)
- [29]. Pili S., Argent S.P., Morris C.G., Rought P., Sakai V., Silverwood I.P., Easun T.L., Li M., Warren M.R., Murray C.A., Tang C.C., Yang S., Schroider M. (2016), Proton Conduction in a Phosphonate-Based

- Metal–Organic Framework Mediated by Intrinsic “Free Diffusion inside a Sphere”, *J Am Chem Soc*, 138, 20, 6352-6355 (DOI: 10.1021/jacs.6b02194)
- [30]. Lea J.D., Lizaran I.O., Sanchez L.F., Alio J.L., Cuenca N., Estrada A.F., Albero J.S. (2019), Metal–Organic Frameworks as Drug Delivery Platforms for Ocular Therapeutics, *ACS Appl Mater Interfaces*, 11, 2, 1924-1931 (DOI: 10.1021/acsami.8b20222)
- [31]. Lei B., Wang M., Jiang Z., Qi W., Su R., He Z. (2018), Constructing Redox-Responsive Metal–Organic Framework Nanocarriers for Anticancer Drug Delivery, *ACS Appl Mater Interfaces*, 10, 19, 16698-16706 (DOI: 10.1021/acsami.7b19693)
- [32]. Wang Li., Zheng M., Xie Z. (2018), Nanoscale metal–organic frameworks for drug delivery: a conventional platform with new promise, *J Mater Chem B*, 6, 707-717 (DOI: 10.1039/C7TB02970E)
- [33]. Wu M., Yang Y. (2017), Metal–Organic Framework (MOF)-Based Drug/Cargo Delivery and Cancer Therapy, *Adv Mater*, 29, 23, 1606134 (DOI: 10.1002/adma.201606134)
- [34]. Simagina A.A., Polynski M.V., Vinogradov A.V., Pidko E.A. (2018), Towards rational design of metal-organic framework-based drug delivery systems, *Russ Chem Rev*, 87, 9, 831-858 (DOI: 10.1070/RCR4797)
- [35]. Ibrahim M., Sabouni R., Hussein G.A. (2017), Anti-cancer Drug Delivery Using Metal Organic Frameworks (MOFs), *Curr Med Chem*, 24, 2, 193-214 (DOI: 10.2174/0929867323666160926151216)
- [36]. Sun Y., Gao J., Cheng Y., Zhang Y., Zeng K. (2019), Design of the Hybrid Metal–Organic Frameworks as Potential Supramolecular Piezo-/Ferroelectrics, *J Phys Chem C*, 123, 5, 3122-3129 (DOI: 10.1021/acs.jpcc.8b08442)
- [37]. Pan L., Liu G., Li H., Meng S., Han L., Shang L., Chen B., Prats A.E.P., Lu W., Zou X., Li R.W. (2014), A Resistance-Switchable and

- Ferroelectric Metal–Organic Framework, *J Am Chem Soc*, 136, 50, 17477-17483 (DOI: 10.1021/ja508592f)
- [38]. Guo P.C., Chu Z., Ren X.M., Ning W.H., Jin W. (2013), Comparative study of structures, thermal stabilities and dielectric properties for a ferroelectric MOF $[\text{Sr}(\mu\text{-BDC})(\text{DMF})]_{\infty}$ with its solvent-free framework, *Dalton Trans*, 42, 6603-6610 (DOI: 10.1039/C3DT32880E)
- [39]. Zhang W., Xiong R.G. (2012), Ferroelectric Metal–Organic Frameworks, *Chem Rev*, 112, 2, 1163-1195 (DOI : 10.1021/cr200174w)
- [40]. Asadi K., Veen M.A. (2016), Ferroelectricity in Metal–Organic Frameworks: Characterization and Mechanisms, *Eur J Inorg Chem*, 27, 4332-4344 (DOI: 10.1002/ejic.201600932)
- [41]. Hijikata Y., Horike S., Sugimoto M., Inukai M., Fukushima T., Kitagawa S. (2013), Pore Design of Two-Dimensional Coordination Polymers toward Selective Adsorption, *Inorg Chem*, 52, 7, 3634-3642 (DOI: 10.1021/ic302006x)
- [42]. Chen C.Y., Cheng P., Wu H., Lee H.M. (2007), Conformational Effect of 2,6-Bis(imidazol-1-yl)pyridine on the Self-Assembly of 1D Coordination Chains: Spontaneous Resolution, Supramolecular Isomerism, and Structural Transformation, *Inorg Chem*, 46, 14, 5691-5699 (DOI: 10.1021/ic700428e)
- [43]. Natarajan K., Gupta A.K., Ansari S.N., Saraf M., Mobin S.M. (2019), Mixed-Ligand-Architected 2D Co(II)-MOF Expressing a Novel Topology for an Efficient Photoanode for Water Oxidation Using Visible Light, *ACS Appl Mater Interfaces*, 11, 14, 13295-13303 (DOI: 10.1021/acsami.9b01754)
- [44]. Ansari S.N., Verma S.K., Garin A.A., Mobin S.M. (2018), Vacuum-Mediated Single-Crystal-to-Single-Crystal (SCSC) Transformation in Na-MOFs: Rare to Novel Topology and Activation

- of Nitrogen in Triazole Moieties, *Crystal Growth & Design*, 18, 3, 1287-1292 (DOI: 10.1021/acs.cgd.7b01753)
- [45]. Sen S., Neogi D., Aijaz A., Xu Q., Bharadwaj P.K. (2014), Construction of Non-Interpenetrated Charged Metal–Organic Frameworks with Doubly Pillared Layers: Pore Modification and Selective Gas Adsorption, *Inorg Chem*, 53, 14, 7591-7598 (DOI: 10.1021/ic500900n)
- [46]. Gupta A.K., De D., Katoch R., Garg A., Bharadwaj P.K. (2017), Synthesis of a NbO Type Homochiral Cu(II) Metal–Organic Framework: Ferroelectric Behavior and Heterogeneous Catalysis of Three-Component Coupling and Pechmann Reactions, *Inorg Chem*, 56, 4697–4705 (DOI: 10.1021/acs.inorgchem.7b00342)
- [47]. Saraf M., Rajak R., Mobin S.M. (2016), A fascinating multitasking Cu-MOF/rGO hybrid for high performance supercapacitors and highly sensitive and selective electrochemical nitrite sensors, *J Mater Chem A*, 4, 16432-16445 (DOI: 10.1039/C6TA06470A)
- [48]. Nagaraju D.H., Wang Q., Beaujuge P., Alshareef H. N. (2014), Two-dimensional heterostructures of V₂O₅ and reduced graphene oxide as electrodes for high energy density asymmetric supercapacitors, *J Mater Chem A*, 2, 17146-17152 (DOI: 10.1039/C4TA03731F)
- [49]. Rajak R., Saraf M., Mobin S.M. (2019), Robust heterostructures of a bimetallic sodium–zinc metal–organic framework and reduced graphene oxide for high-performance supercapacitors, *J Mater Chem A*, 7, 1725-1736 (DOI: 10.1039/C8TA09528K)
- [50]. Gong Y., Li J., Jiang P., Li Q., Lin J. (2013), Novel metal(II) coordination polymers based on N,N'-bis-(4-pyridyl)phthalamide as supercapacitor electrode materials in an aqueous electrolyte, *Dalton Trans*, 42, 1603-1611 (DOI: 10.1039/c2dt31965a)
- [51]. Du M., Chen M., Yang X., Wen J., Wang X., Fang S., Liu C. (2014), A channel-type mesoporous In(III)–carboxylate coordination

- framework with high physicochemical stability for use as an electrode material in supercapacitors, *J Mater Chem A*, 2, 9828-9834 (DOI: 10.1039/C4TA00963K)
- [52]. Zhang D., Shi H., Zhang R., Zhang Z., Wang N., Li J., Yuan B., Bai H., Zhang J. (2015), Quick synthesis of zeolitic imidazolate framework microflowers with enhanced supercapacitor and electrocatalytic performances, *RSC Adv*, 5, 58772-58776 (DOI: 10.1039/C5RA08226A)
- [53]. Lee D.Y., Shinde D.V., Kim E.K., Lee W., Oh I.W., Shrestha N.K., Lee J.K., Han S.H. (2013), Supercapacitive property of metal-organic-frameworks with different pore dimensions and morphology, *Microporous and Mesoporous Mater*, 171, 53-57 (DOI: 10.1016/j.micromeso.2012.12.039)
- [54]. Diaz R., Orcajo M.J., Botas J.A., Calleja G., Palma J. (2012), Co8-MOF-5 as electrode for supercapacitors, *Materials Letters*, 68, 126-128 (DOI: 10.1016/j.matlet.2011.10.046)
- [55]. Ramachandran R., Xuan W., Zhao C., Leng X., Sun D., Luo D., Wang F. (2018), Enhanced electrochemical properties of cerium metal-organic framework based composite electrodes for high-performance supercapacitor application, *RSC Adv*, 8, 3462-3469 (DOI: 10.1039/C7RA12789H)
- [56]. Srimuk P., Luanwuthi S., Krittayavathananon A., Sawangphruk M. (2015), Solid-type supercapacitor of reduced graphene oxide-metalorganic framework composite coated on carbon fiber paper, *Electrochimica Acta*, 157, 69-77 (DOI: 10.1016/j.electacta.2015.01.082)

